

# Chasing the Chelyabinsk asteroid $N$ -body style

C. de la Fuente Marcos and R. de la Fuente Marcos

*Apartado de Correos 3413, E-28080 Madrid, Spain*

carlosdlfmarcos@gmail.com

and

S. J. Aarseth

*Institute of Astronomy, University of Cambridge, Madingley Road, Cambridge CB3 0HA, UK*

## ABSTRACT

On 2013 February 15 a small asteroid rammmed against the atmosphere above the region of Chelyabinsk in Russia, producing the most powerful superbolide since the Tunguska event in 1908. Lacking proper astrometric observations, the pre-impact orbit of this object has been determined using videos, satellite images, and pure geometry. Unfortunately, more than two years after the event, the published estimates vary so much that there is no clear orbital solution that could be used to investigate the origin of the impactor and the existence of dynamically, or perhaps even genetically, related asteroids. Here, we revisit this topic using a full  $N$ -body approach. A robust statistical test is applied to published solutions to discard those unable to produce a virtual impact at the observed time ( $03:20:20.8 \pm 0.1$  s UTC). The same  $N$ -body methodology and the latest ephemerides are used to compute a new orbital solution:  $a = 1.6247$  AU,  $e = 0.5318$ ,  $i = 3^\circ.9750$ ,  $\Omega = 326^\circ.4607$  and  $\omega = 109^\circ.7012$ . This new solution—which has an impact probability  $> 0.99999$  and uncertainties in time and space of 0.2 s and 6 km, respectively—is utilized to explore the past orbital evolution of the impactor as well as the presence of near-Earth objects moving in similar paths. A dynamical link between asteroid 2011 EO<sub>40</sub> and the Chelyabinsk impactor is confirmed. Alternative orbital solutions are extensively explored.

*Subject headings:* celestial mechanics – meteorites, meteors, meteoroids – methods: statistical – minor planets, asteroids: general – minor planets, asteroids: individual (2011 EO<sub>40</sub>) – planets and satellites: individual (Earth)

## 1. Introduction

Asteroids diving out of the Sun’s blinding glare represent a very real threat that cannot be easily detected or defended against with currently available resources. In general, any minor body

that encounters our planet after reaching perihelion inside the orbit of the Earth will approach undetected, hidden in the daytime sky. If the true minimal approach distance to our planet is small enough (e.g.,  $<0.001$  AU) this configuration is sometimes described as the Red Baron dynamical scenario (Adamo 2011), in which the glare of the Sun provides an effective hiding spot to a close passage or an eventual impactor. The most dramatic recent example of such an occurrence was the Chelyabinsk event.

On 2013 February 15 a small asteroid approached the Earth undetected, coming from the direction of the Sun, and slammed against the atmosphere above the region of Chelyabinsk in Russia, producing the most powerful superbolide since the Tunguska event in 1908 (Brown et al. 2013; Le Pichon et al. 2013). In the absence of pre-impact astrometric observations, the orbit followed by the parent body of the Chelyabinsk superbolide has been determined using videos recorded by witnesses (Borovička et al. 2013; Popova et al. 2013; Zuluaga et al. 2013; Emel’Yanenko et al. 2014; Dmitriev et al. 2015; Golubaev 2015), satellite images (Proud 2013), and pure geometry (de la Fuente Marcos & de la Fuente Marcos 2013, 2014; hereinafter Papers I and II, respectively). Unfortunately, more than two years after the event, the published estimates vary so much that there is no clear orbital solution that could be used to investigate the origin of the impactor and the existence of dynamically and/or physically related asteroids.

The notion of pre-impact orbit is widely used in the study of cosmic strikes, but, what is the pre-impact orbit of the parent body of a meteor? The most natural answer to this non-trivial question would be that it is the one computed for an epoch sufficiently distant from the impact time and such that its subsequent evolution produces an impact within a reasonable time frame imposed by the available observational data. Such an accurate orbital solution is appropriate to study both the past dynamical evolution of the parent body of the meteor and the possible existence of other small bodies moving in similar orbits among known near-Earth objects (NEOs). No matter the methodology behind a given orbital solution, it must comply with the hard experimental evidence: impact time and location. Orbital solutions must be rejected on the grounds of their failure to generate an impact at the correct time on the right spot. In the case of the Chelyabinsk superbolide, it was first detected on 2013 February 15 03:20:20.8 $\pm$ 0.1 s UTC ( $t_{\text{impact}}$ ) at longitude 64°565 $\pm$ 0°030 ( $\lambda_{\text{impact}}$ ), latitude +54°445 $\pm$ 0°018 ( $\phi_{\text{impact}}$ ) and altitude 97.1 $\pm$ 0.7 km (see Table S1, Popova et al. 2013, also Borovička et al. 2013; Miller et al. 2013).

Here, we revisit the topic of the pre-impact orbit of the Chelyabinsk superbolide using a full  $N$ -body methodology to both rank the published solutions and obtain a new one. This paper is organized as follows. The published orbits are briefly discussed in Section 2. In Section 3, a statistically robust impact test is described, validated, and applied to published orbital solutions. Our full  $N$ -body approach is presented in Section 4. A new pre-impact orbit is derived in Section 5; alternative orbital solutions are also extensively explored there. This new orbital solution is used in Section 6 to study the past dynamical evolution of the Chelyabinsk impactor and investigate the presence of known NEOs moving in similar orbits. Results are discussed and conclusions summarized in Section 7.

## 2. The pre-impact orbit so far

More or less detailed orbital solutions have been presented in Adamo (2013), Borovička et al. (2013), Chodas & Chesley,<sup>1</sup> Dmitriev et al. (2015), Emel’Yanenco et al.,<sup>2</sup> Emel’Yanenko et al. (2014), Golubaev (2015), Green (2013), Lyytinen,<sup>3</sup> Lyytinen et al.,<sup>4</sup> Nakano,<sup>5</sup> Popova et al. (2013), Proud (2013), Zuluaga & Ferrin,<sup>6</sup> Zuluaga et al. (2013),<sup>7</sup> and Papers I and II. The vast majority of these solutions have been obtained from videos recorded by witnesses, but satellite images (Proud 2013) and pure geometry (Papers I and II) have also been used. All of them show that the dynamical class of the Chelyabinsk impactor is Apollo and the impact occurred at the descending node, but the actual values of the orbital elements are still under dispute (see Table 1 for values of semimajor axis,  $a$ , eccentricity,  $e$ , inclination,  $i$ , longitude of the ascending node,  $\Omega$ , argument of perihelion,  $\omega$ , and time of perihelion passage,  $\tau$ ; the rest can be found in Papers I and II). The relative dispersion between solutions is large enough to make them incompatible: 10.9% in  $a$ , 9.3% in  $e$ , 25.4% in  $i$ , 0.025% in  $\Omega$ , and 6.4% in  $\omega$ . In the following, we apply a new technique—using full  $N$ -body calculations—to test published orbital determinations statistically and derive a robust solution.

---

<sup>1</sup>[http://neo.jpl.nasa.gov/news/fireball\\_130301.html](http://neo.jpl.nasa.gov/news/fireball_130301.html)

<sup>2</sup>[http://www.inasan.ru/eng/asteroid\\_hazard/chelyabinsk\\_bolid\\_new.html](http://www.inasan.ru/eng/asteroid_hazard/chelyabinsk_bolid_new.html)

<sup>3</sup><http://www.amsmeteors.org/2013/02/large-daytime-fireball-hits-russia/>

<sup>4</sup><http://www.projectpluto.com/temp/chelyab.htm>

<sup>5</sup><http://www.icq.eps.harvard.edu/CHELYABINSK.HTML>

<sup>6</sup><http://arxiv.org/abs/1302.5377>

<sup>7</sup><http://astronomia.udea.edu.co/chelyabinsk-meteoroid/>

Table 1: Published Solutions for the Pre-impact Orbit of the Chelyabinsk Impactor

Authors	$a$ (AU)	$e$	$i$ (deg)	$\Omega$ (deg)	$\omega$ (deg)	$\tau$ (JDCT)	$P_{\text{imp}}$
Green (2013)	1.55±0.07	0.50±0.02	3.6±0.7	326.410±0.005	109.7±1.8	–	–
Borovička et al. (2013)	1.72±0.02	0.571±0.006	4.98±0.12	326.459±0.001	107.67±0.17	2456292.89±0.17	$\leq 10^{-5}$
Dmitriev et al. (2015)	1.76±0.04	0.580±0.012	5.0±0.3	326.454±0.002	108.2±0.7	–	–
Emel'Yanenko et al. (2014)	1.88±0.07	0.609±0.017	5.9±0.4	326.446±0.002	108.9±0.5	2456294.4±5.4	$< 10^{-6}$
Golubaev (2015)	1.67±0.10	0.57±0.03	7.1±0.5	326.42	106.3±2.5	–	–
Paper I	1.62375±0.00014	0.53279±0.00011	3.817±0.005	326.4090±0.0007	109.44±0.03	2456292.478±0.005	$\leq 0.005$
Paper II	1.624765±0.000005	0.53184±0.00001	3.97421±0.00005	326.44535±0.00001	109.71442±0.00004	2456292.57800±0.00004	$\leq 0.77$
Popova et al. (2013)	1.76±0.08	0.581±0.009	4.93±0.24	326.4422±0.0014	108.3±1.9	2456293.4±2.0	$\leq 10^{-6}$
Proud (2013)	1.47 <sup>+0.03</sup> <sub>-0.13</sub>	0.52 <sup>+0.01</sup> <sub>-0.05</sub>	4.61 <sup>+2.58</sup> <sub>-2.09</sub>	326.53 <sup>+0.01</sup> <sub>-0.0</sub>	96.58 <sup>+2.94</sup> <sub>-1.72</sub>	–	–
Zuluaga & Ferrin <sup>6</sup>	1.73±0.23	0.51±0.08	3.45±2.02	326.70±0.79	120.62±2.77	–	–
Zuluaga et al. (2013)	1.27±0.05	0.44±0.02	3.0±0.2	326.54±0.08	95.1±0.8	–	–
Zuluaga et al. <sup>7</sup>	1.368±0.006	0.470±0.010	4.0±0.3	326.479±0.003	99.6±1.3	–	–
Average± $\sigma$	1.6±0.2	0.53±0.05	4.5±1.1	326.48±0.08	107±7	2456293.1±0.4	
This work	1.62470348	0.53184268	3.9749908	326.4607324	109.7012184	2456292.5834112	
	±	±	±	±	±	±	>0.99999
	0.00000005	0.00000002	0.0000008	0.0000014	0.0000008	0.0000010	

Note. The errors from Popova et al. (2013) are from their Table S5B.  $P_{\text{imp}}$  is the impact probability. Paper I is de la Fuente Marcos & de la Fuente Marcos (2013). Paper II is de la Fuente Marcos & de la Fuente Marcos (2014).

### 3. Orbit validation: impact test

Independently from the methodology used to derive it, any computed orbit must be consistent with the well-established fact that a superbolide was observed on 2013 February 15 03:20:20.8±0.1 s UTC at longitude 64°565±0°030, latitude +54°445±0°018, and altitude 97.1±0.7 km (see Table S1, Popova et al. 2013). Our solution in Paper II satisfies these constraints relatively well, but it was referred to an epoch arbitrarily close to that of the impact event; therefore, it does not describe the pre-impact orbit of the Chelyabinsk impactor in a strict sense. The same can be said about other published solutions.

#### 3.1. Method

The robust statistical impact test described in this section can be viewed as an independent implementation of the ideas explored in Sitarski (1998, 1999, 2006).<sup>8</sup> In his work, Sitarski uses pre-impact observational information as input to develop his methodology to predict asteroid impacts. Any asteroid’s full orbital solution can be used to generate synthetic observational data suitable to be tested for virtual impacts or close encounters with our planet or any other body in the solar system. The approach is very simple; we assume a set of orbital elements ( $a$ ,  $e$ ,  $i$ ,  $\Omega$ ,  $\omega$ , and  $\tau$ ) at a given epoch  $t_0$ , generate Cartesian state vectors ( $\mathbf{r}$  and  $\mathbf{v}$ ) for the assumed orbit at the reference epoch, and use  $N$ -body simulations within a certain physical model to study the evolution of the assumed orbit until an impact or a miss occurs. If a large sample of orbits is studied, the conventional statistical analysis of their outcomes in the form of frequency histograms (for  $t_{\text{impact}}$  and other parameters) should be enough to decide if a candidate impact orbit is statistically robust or not. In our case, a Monte Carlo approach (Metropolis & Ulam 1949; Press et al. 2007) is used to generate sets of orbital elements. Unless explicitly stated, Gaussian random numbers are utilized to emulate better the results from traditional, astrometry-based orbital solutions; the Box-Muller method is applied to generate random numbers with a normal distribution (Press et al. 2007).

Our model solar system includes the perturbations from the eight major planets and treats the Earth and the Moon as two separate bodies. It also incorporates the barycenter of the dwarf planet Pluto–Charon system and the five most massive asteroids of the main belt, namely, (1) Ceres, (2) Pallas, (4) Vesta, (10) Hygiea, and (31) Euphrosyne. Using a different number of perturbing asteroids has no impact on most of our results (impact tests and pre-impact orbit determinations). However, a small but measurable variation is found when investigating the past evolution of the various objects studied here for the time interval considered; the variations are too small to affect any of our conclusions. We use initial conditions (positions and velocities referred to the barycenter of the solar system) provided by the Jet Propulsion Laboratory (JPL) HORIZONS system (Giorgini et al. 1996; Standish 1998) and relative to the Julian Date 2456337.638888889 (= A.D. 2013

---

<sup>8</sup><http://phas.cbk.waw.pl/neo.htm>

February 14 03:20:00.0000), Coordinate Time (JDCT) epoch ( $t_0$ ,  $t = 0$  in the figures, see Table 9), i.e., the integrations are started  $\sim 24$  hr before  $t_{\text{impact}}$ . We retain the level of precision in time ( $\sim 0.0001$  s) provided by the HORIZONS system throughout the paper. Cartesian state vectors for the test orbits are generated using the Monte Carlo technique pointed out above, within some given or assumed ranges for the orbital parameters, and the usual expressions in, e.g., Murray & Dermott (1999). The  $N$ -body simulations performed here were completed applying the Hermite integration scheme described by Makino (1991) and implemented by Aarseth (2003). The standard version of this direct  $N$ -body code is publicly available from the IoA web site.<sup>9</sup> Non-gravitational forces, relativistic and oblateness terms are not included in the calculations; additional details can be found in de la Fuente Marcos & de la Fuente Marcos (2012), where the results of this  $N$ -body code are compared with those from other codes as well. For the case studied here, the role of the Earth’s oblateness is rather negligible —see the analysis in Dmitriev et al. (2015). Relative errors in the total energy are as low as  $10^{-14}$  to  $10^{-13}$  or lower. The relative error in the total angular momentum is several orders of magnitude smaller.

In the particular problem that we are considering here, our choice of  $t_0$  places the impactor near the edge of the Hill sphere of the Earth (0.0098 AU) at the beginning of the simulation (0.008 AU) and results in a systematic difference at the end of the integration, between our ephemerides and those provided by the JPL for the Earth, of about 6 km. As the average orbital speed of our planet is  $29.78 \text{ km s}^{-1}$ , it implies that the temporal systematic error in our impact calculations could be as small as 0.2 s, which matches well the actual uncertainty in  $t_{\text{impact}}$ . In comparison, the time taken by our planet to travel a distance equal to its own average diameter (12,742 km,  $R_E = 6371$  km) is nearly 7.1 minutes. A spatial error of 6 km is equivalent to an angular error of  $0^\circ.054$  in geographical coordinates that also parallels the level of angular precision in  $\lambda_{\text{impact}}$  and  $\phi_{\text{impact}}$ . Therefore, our results are as realistic as they can possibly be within the known observational uncertainties.

The very precise values of the impact parameters available for this particular impact event impose very tight limits on the maximum values of the systematic errors that can be tolerated during the integrations in order to obtain statistically meaningful results. For example, if the value of the integration errors in the position of the Earth at the end of the simulations is of the order of a few hundred kilometers, this is equivalent to an error in the angular quantities  $> 1^\circ$  and therefore more than 30 times the largest deviation in impact coordinates; such a scenario is completely unacceptable under the present circumstances and cannot lead to any usable results. This important issue has been neglected in the published literature on this subject although it is of the utmost importance in this particular case.

---

<sup>9</sup><http://www.ast.cam.ac.uk/~sverre/web/pages/nbody.htm>

### 3.2. Quality control: the case of Duende

Before applying the  $N$ -body-based statistical test to any solution, one key question must be answered: How reliable is the test? Can we trust its results? Perhaps it includes some kind of unknown systematics that may favor some solutions over others or, as pointed out above, the computational errors are large enough to produce inconclusive results. Synthetic data, generated under controlled conditions, are often used to validate statistical tests before applying them to real data. In our case, this approach may add more sources of uncertainty as the test itself rests on generating a very large amount of synthetic data (but nonetheless based on observational data). Being able to test our approach with data coming from a well-studied real event would be far more advantageous.

Fortunately or not, the Chelyabinsk event was not the only spectacular cosmic event that took place on 2013 February 15: asteroid 367943 Duende (2012 DA<sub>14</sub>) passed nearly 27,700 km above the Earth’s surface, well inside the boundaries of the ring of geosynchronous satellites although almost perpendicular to it, reducing the chances of an actual collision with one of them. This rather unusual episode had been expected for about a year (see, e.g., Wlodarczyk 2012) and it was followed closely by the scientific community worldwide (see, e.g., de León et al. 2013; Nechaeva et al. 2013; Terai et al. 2013; Urakawa et al. 2013; Takahashi et al. 2014). While waiting for this close encounter to happen, the Chelyabinsk event took place. The evidence compiled so far indicates that the two events were completely independent and unrelated.

Duende was closest to the Earth on February 15 at approximately 19:25:49.4 UTC ( $t_{\text{close}} = 2456339.309600038 \pm 0.000000120$  JDCT), 27,679 $\pm$ 15 km above the Earth’s surface.<sup>10, 11</sup> At the time of closest approach, the asteroid flew over the eastern Indian Ocean,  $\lambda \sim 97^\circ 5$  E and  $\phi \sim 6^\circ$  S, off the Indonesian island of Sumatra. In order to try to reproduce these close encounter parameters (and their errors) derived by the JPL’s Solar System Dynamics Group (SSDG), we use the tools and numerical model described above and analyze the results. In principle, the orbital elements of the test orbits can be obtained by varying them randomly, within the ranges defined by their mean values and standard deviations (i.e., as provided by the HORIZONS system). For example, a new value of the orbital inclination can be found using the expression  $i_t = \langle i \rangle + \sigma_i r_i$ , where  $i_t$  is the inclination of the test orbit,  $\langle i \rangle$  is the mean value of the inclination (candidate pre-impact orbit or full orbit from the HORIZONS system),  $\sigma_i$  is the standard deviation of  $i$ , and  $r_i$  is a (pseudo) random number with normal distribution in the range  $-1$  to  $1$ . Sitarski (1998, 1999, 2006) has pointed out that this is equivalent to considering a number of different virtual minor planets moving in similar orbits, but not a sample of test orbits incarnated from a set of observations obtained for a single minor planet. The orbit of Duende has been computed from a set of observations and, therefore, applying the classical —but statistically wrong— expressions may lead to unphysical results. The

---

<sup>10</sup><http://www.nasa.gov/topics/solarsystem/features/asteroidflyby.html>

<sup>11</sup><http://ssd.jpl.nasa.gov/sbdb.cgi?sstr=2012DA14;cad=1#cad>

correct statistical alternative is to consider how the elements affect each other, applying the Monte Carlo using the Covariance Matrix (MCCM) approach (Bordovitsyna et al. 2001; Avdyushev & Banschikova 2007), or to follow the procedure described in Sitarski (1998, 1999, 2006).

Figure 1 displays the results of a set of  $10^5$  numerical experiments using initial conditions generated by applying the classical but wrong approach that neglects the covariance matrix. It is clear that the integrations reproduce the data obtained by the SSDG but the dispersions are rather large. To further explore this remarkable close encounter, we have used an implementation of the MCCM approach (for full mathematical details see Section 3 in de la Fuente Marcos & de la Fuente Marcos 2015); i.e., a Monte Carlo process creates test orbits with initial parameters from the nominal orbit (for the  $t_0$  epoch), adding random noise on each initial orbital element and making use of the covariance matrix. The results for this new set of  $10^5$  numerical experiments are presented in Figure 2. Consistently with Figure 5 in Sitarski (1998), the outcomes from these two approaches are very different but nonetheless statistically compatible. The difference between our value for the time of closest approach (2456339.309607290 JDCT) using MCCM and the one determined by the SSDG is 0.627 s, and that of the distance of closest approach (27,681.80 km) is 2.9 km. Regarding the relative velocity at closest approach, the value quoted by the SSDG (no errors) is  $7.81996942783692 \text{ km s}^{-1}$  and the one from our MCCM approach is  $7.8199012 \pm 0.0000007 \text{ km s}^{-1}$ . In this and future calculations the error quoted is the standard deviation ( $1\sigma$ ) unless explicitly stated. These results match the level of precision required to conduct the statistical test discussed in the previous section. The methodology described above is robust enough to provide objective and reliable results. If any of the tested solutions is unable to generate virtual impacts consistent with the observational data, this will not be due to the test itself, but because the actual pre-impact candidate orbital solution is incorrect. In this context, any solution giving a reasonable fraction of impacts with parameters within the observational uncertainties can be considered as a robust pre-impact orbital solution.

### 3.3. Impact test: results

In order to assess the suitability of a given solution by applying the methodology described in the previous sections, we require the entire set of six orbital elements and their standard deviations, which are only readily available for the orbital solutions presented in Borovička et al. (2013) and Popova et al. (2013). These two solutions are regarded by many as the best determinations published so far (but see Paper II, which presents a different statistical test that is applied to most of the orbital solutions in Table 1). For these orbital solutions and the one in Emel’Yanenko et al. (2014) —which is presented as an improvement with respect to Popova et al. (2013)— we have studied the evolution of  $10^6$  test orbits from  $t_0$  until some time after  $t_{\text{impact}}$  using the scheme outlined above. The orbital elements of the test orbits for a given orbital solution have been computed, varying them randomly, within the ranges defined by their mean values and standard deviations (see Table 1) as described above. No covariance matrices have been used in these tests

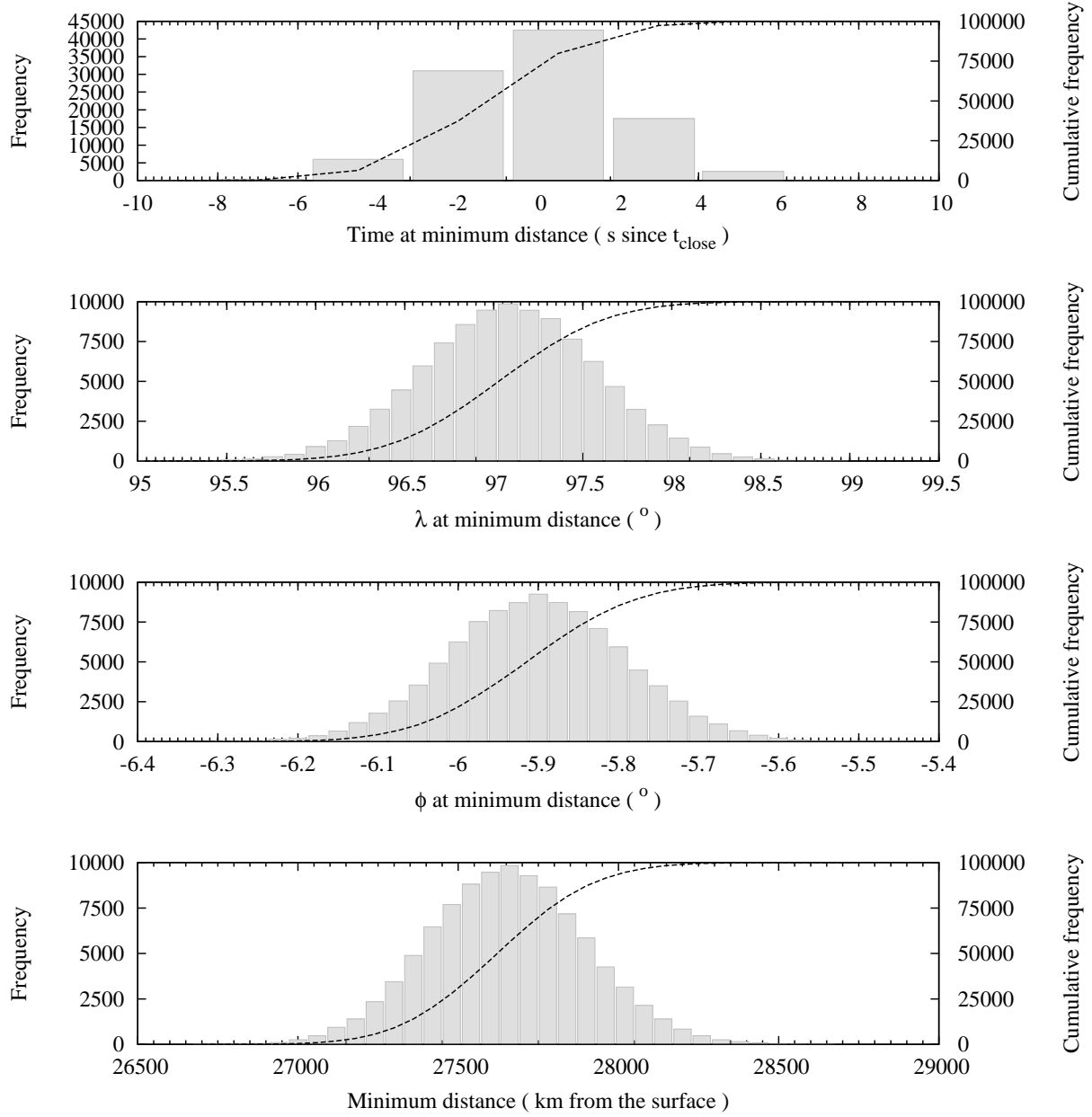


Fig. 1.— Parameters of the close encounter with 367943 Duende (2012 DA<sub>14</sub>) on 2013 February 15 for a set of  $10^5$  numerical experiments using initial conditions generated by applying the classical approach described in the text. The value of  $t_{\text{close}}$  as determined by the JPL’s SSDG is  $2456339.309600038 \pm 0.000000120$  JDCT at a minimum distance of  $27,679 \pm 15$  km above the Earth’s surface. The number of bins in the top panel is small because of the unavoidable discretization of the output interval.

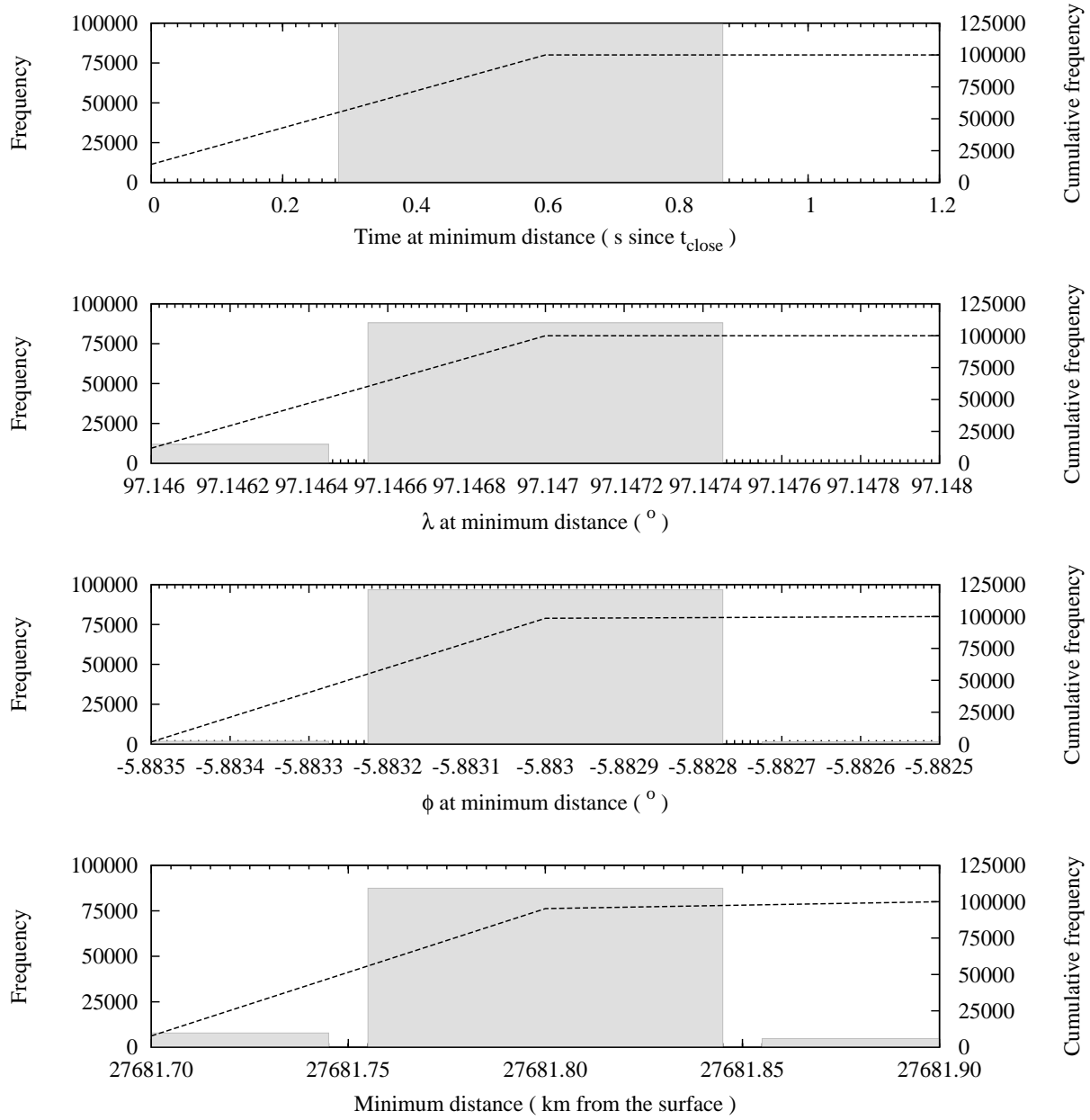


Fig. 2.— Same as Figure 1 but for numerical experiments using initial conditions generated by applying the covariance matrix (see the text for details). The bins are few because the values of the dispersions are very small and due to the unavoidable discretization of the output interval. The difference between our value for the time of closest approach and the one determined by the JPL’s SSDG is 0.627 s and that of the distance of closest approach is 2.9 km. These values are consistent with the level of precision required to conduct the statistical test discussed in the text.

because none has been included among the results published so far. The only differences between the computations described here and those carried out for Duende in the previous section are in the input average values and their standard deviations (see Table 1) for the various orbital elements, and in the fact that the simulated time in the case of Duende is nearly 16 hr longer.

The input orbital elements and the results of these simulations are plotted in Figures 3 and 4. The solution in Borovička et al. (2013) is slightly better than the one in Popova et al. (2013) as its impact probability,  $P_{\text{imp}}$ , is  $\leq 10^{-5}$ , about ten times higher than that of the other one (see Table 1). The value of the impact probability has been obtained in the usual way, dividing the number of relevant events by the total number of test orbits studied. The dispersions in both  $t_{\text{impact}}$  and minimal approach distance are very wide. Most calculated close approaches take place well after or before  $t_{\text{impact}}$ . No impacts at the right coordinates were recorded in our numerical experiments. The closest virtual impact (found for the one in Borovička et al. 2013) took place almost 15 minutes after  $t_{\text{impact}}$  at coordinates (69°4 E, 42°4 N) in Kazakhstan:  $a = 1.735709580$  AU,  $e = 0.575817480$ ,  $i = 4.875268780$ ,  $\Omega = 326.460412000$ ,  $\omega = 107.626661600$ , and  $\tau = 2456293.019210$  JDCT (the tabulated precision is intended to facilitate verification). It is perhaps worth mentioning here that a difference in  $t_{\text{impact}}$  of 15 minutes is far from trivial because it is equivalent to over two Earth diameters in terms of space as our planet travels a distance equal to its own average diameter in nearly 7.1 minutes. The results of this independent statistical test are fully consistent with those presented in Paper II. Applying the same test to the solution in Emel’Yanenko et al. (2014), we found that it is even less satisfactory, statistically speaking (see Figures 4 and 5), than the one in Popova et al. (2013).

In Papers I and II, the orbital solutions were derived using a geometric Monte Carlo approach. Such a technique is relatively inexpensive in computational terms and it is able to produce reasonably precise results using very few input data, but the computed solution is not a true pre-impact orbit in the sense explained above. Applying an impact test —analogous to the one used above— to the orbital solution presented in Paper II, we obtain  $P_{\text{imp}} \leq 0.77$  and the virtual impacts take place 8–15 minutes before  $t_{\text{impact}}$  with a range in longitude of (31,  $-75$ )° and latitude of (24, 79)°.

#### 4. Chasing impactors $N$ -body style

The full  $N$ -body statistical test applied in the previous section is certainly robust enough to show that a candidate solution must be incorrect. This technique is particularly well suited to be used within the framework of the inverse problem paradigm in which one starts with the results (the impact parameters) and then calculates the cause (the pre-impact orbit of the impactor). In contrast, the approach followed by Sitarski (1998, 1999, 2006) is that of a forward problem: the causes are known (astrometric observations of a putative impactor) and then the results are computed (if an impact is possible, try to find out when and where). In this context, the approach developed in this section can be seen as a generalization of the techniques explored in Sitarski (1998, 1999, 2006); he uses the pre-impact information as input to develop his methodology to

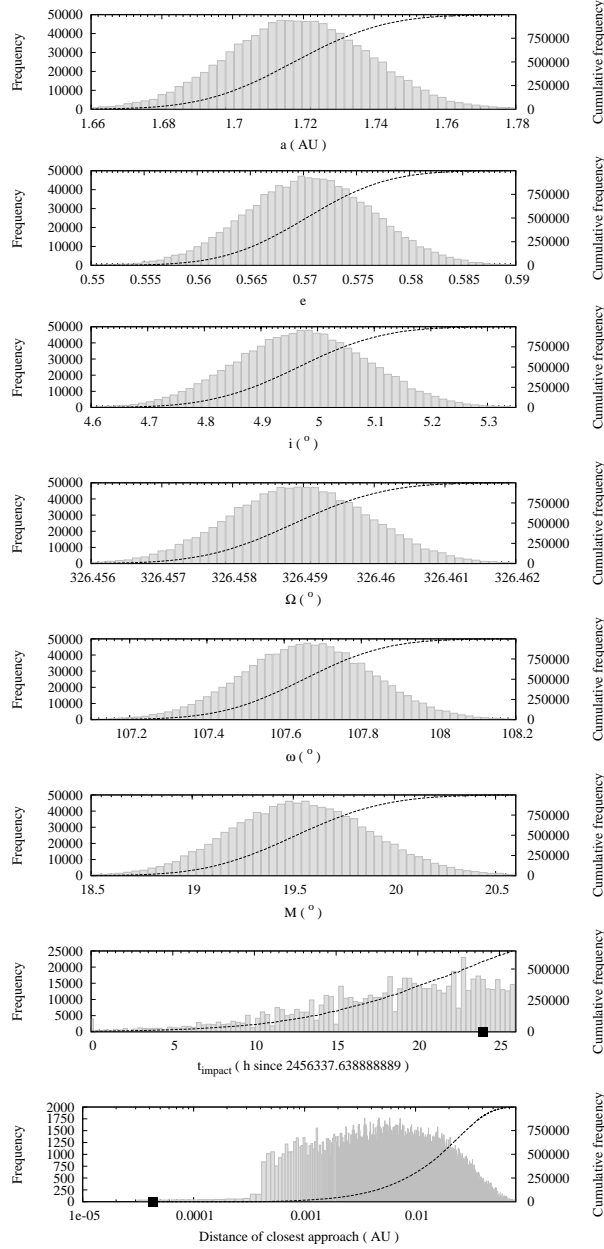


Fig. 3.— Distribution in orbital parameter space for an experiment using the orbital solution presented in Borovička et al. (2013); the impact time ( $\sim 24$  hr after  $t = 0$ ) according to Popova et al. (2013) and the upper atmosphere limit (115 km) are indicated as black squares. This figure is the result of the evolution of  $10^6$  test orbits. The resulting distributions in impact/close-encounter parameter space are displayed in the bottom and second-to-bottom panels. Nearly 30% of the test orbits reach their minimal distance to our planet at the end of the integration; this is why that fraction is missing from the cumulative distribution in the impact time panel. The first six panels provide the input distributions.

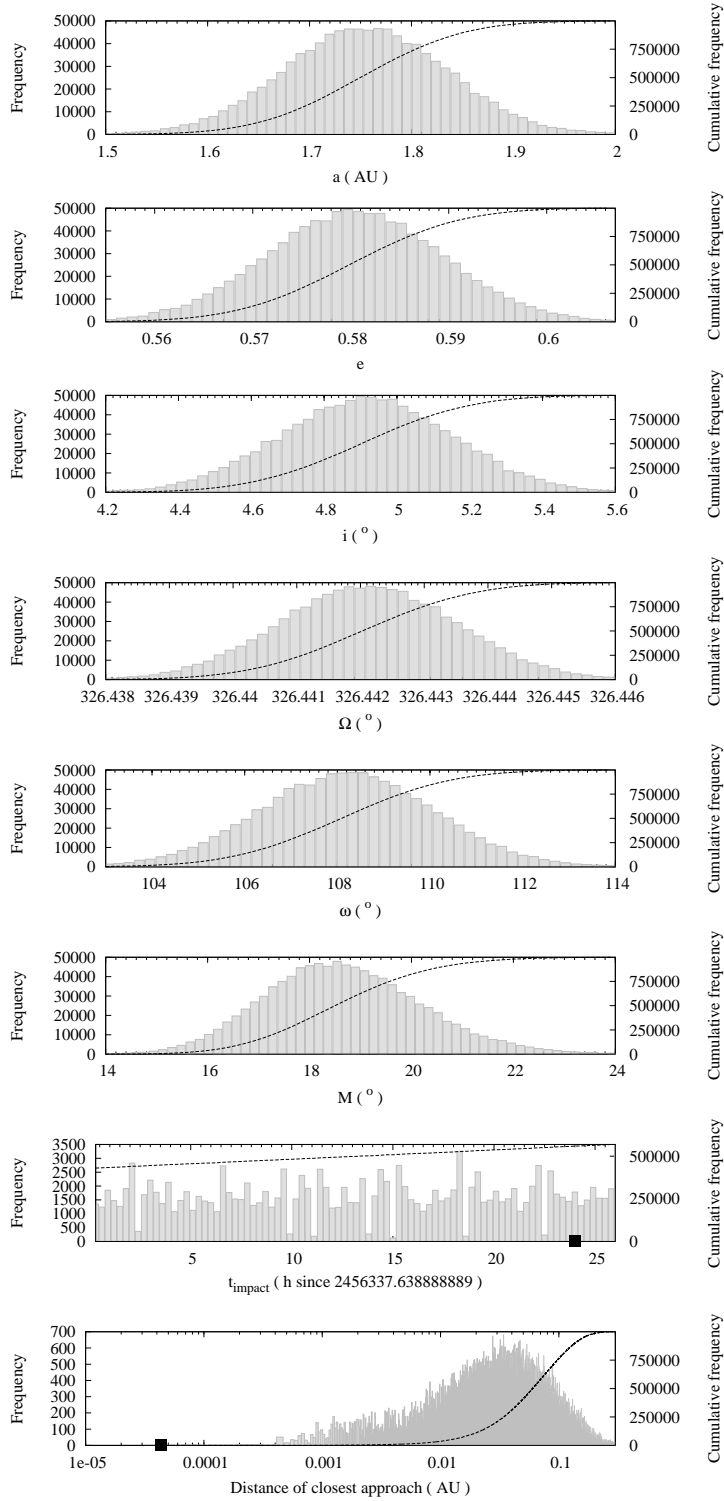


Fig. 4.— Outcome of an experiment similar to that in Figure 3 but for the orbital solution described in Popova et al. (2013). Only about 10% of the orbits tested reach their minimal distance to the Earth during the time interval displayed in the impact time panel.

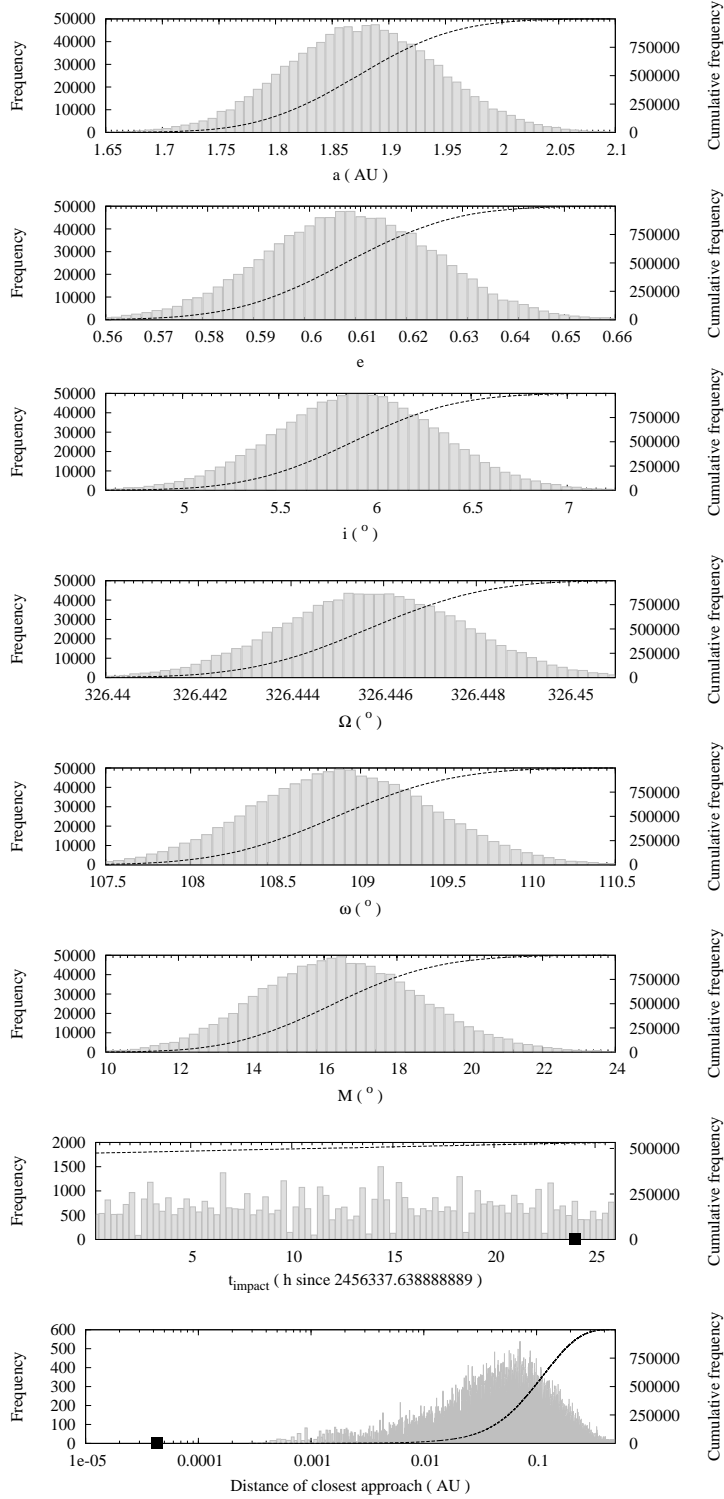


Fig. 5.— Outcome of an experiment similar to that in Figure 3 but for the orbital solution described in Emel’Yanenko et al. (2014). A very small fraction of the orbits tested reach their minimal distance to the Earth during the time interval displayed in the impact time panel.

predict asteroid impacts, but here our goal is to reconstruct the causal factors (the pre-impact orbit) that triggered the observed impact using the post-impact data as a starting point. In inverse problem parlance, we are facing a nonlinear inverse problem in which we know the data (observed impact parameters) and we look for the best model parameters (the orbit) such as the governing equations (the full  $N$ -body treatment) —or forward operator— provide the optimal relationship between model and data (see, e.g., Press et al. 2007).

Most inverse problems are undetermined as the solutions are degenerate, i.e., not unique, with fewer equations than unknowns. It may be argued that the type of inverse problem studied here (going from impact to orbit) cannot be solved because we seek six unknowns (the set of orbital elements) and the post-impact data are just three quantities  $t_{\text{impact}}$ ,  $\lambda_{\text{impact}}$ , and  $\phi_{\text{impact}}$ . However, we also have  $h_{\text{impact}}$ , an estimate of the value of the velocity at  $h_{\text{impact}}$ ,  $v_{\text{impact}}$ , and the standard deviations of all these quantities. On the other hand, it is a well known fact used in probabilistic curve reconstruction (see, e.g., Unnikrishnan et al. 2006, 2010; Unnikrishnan 2008) that if a curve is smooth, the scatter matrix will be elongated and that its major axis, or principal eigenvector, will approximate the direction of the local tangent. It is not unreasonable to assume that the impact trajectory (the pre-impact orbit of the parent body of the superbolide) is smooth in the neighborhood of the impact point (high in the atmosphere) and therefore that the dispersions in  $\lambda_{\text{impact}}$ ,  $\phi_{\text{impact}}$ , and  $h_{\text{impact}}$  provide an appropriate approximation to the local tangent (and indirectly to the instantaneous value of the velocity and its direction) because the principal eigenvector of the data scatter matrix (that contains the values of the variances) is aligned with the true tangent to the impact curve. In this mathematical context our inverse problem may be viable and a solution could be found. In particular, if the available determination of  $v_{\text{impact}}$  is robust then the solution of the inverse problem is strictly unique.

The practical implementation of the solution to this inverse problem requires the use of Monte Carlo techniques (Metropolis & Ulam 1949). As in the previous section, we assume a set of orbital elements ( $a$ ,  $e$ ,  $i$ ,  $\Omega$ ,  $\omega$ , and  $\tau$ ) at a given epoch  $t_0$ , generate Cartesian state vectors ( $\mathbf{r}$  and  $\mathbf{v}$ ) for the assumed orbit at the reference epoch, and use  $N$ -body simulations within the same physical model applied above to study the evolution of the assumed orbit until an impact or a miss occurs. In order to rank the computed solution —if it results in a virtual impact— we use  $t_{\text{impact}}$ ,  $\lambda_{\text{impact}}$ , and  $\phi_{\text{impact}}$ , and a trivariate Gaussian distribution:

$$\Psi = e^{-\frac{1}{2} \left[ \left( \frac{\lambda - \lambda_{\text{impact}}}{\sigma_{\lambda_{\text{impact}}}} \right)^2 + \left( \frac{\phi - \phi_{\text{impact}}}{\sigma_{\phi_{\text{impact}}}} \right)^2 + \left( \frac{t - t_{\text{impact}}}{\sigma_{t_{\text{impact}}}} \right)^2 \right]}, \quad (1)$$

where  $\lambda$  and  $\phi$  are the impact coordinates,  $t$  is the impact time for the assumed test orbit, and  $\sigma_{\lambda_{\text{impact}}}$ ,  $\sigma_{\phi_{\text{impact}}}$ , and  $\sigma_{t_{\text{impact}}}$  are the standard deviations associated with  $\lambda_{\text{impact}}$ ,  $\phi_{\text{impact}}$ , and  $t_{\text{impact}}$ , respectively, supplied with the observational impact values. The closer the value of  $\Psi$  to 1, the better. The functional form of  $\Psi$  assumes that there is no correlation between  $\lambda$ ,  $\phi$ , and  $t$ . In our implementation,  $\Psi$  is our objective function and our algorithm usually converges after exploring several million orbits. Seeking the optimal orbit can be (and it was) automated using a feedback loop to accelerate convergence in real time. If enough test orbits are studied, the

best pre-impact orbit can be determined. This assumption is based on the widely accepted idea that statistical results of an ensemble of collisional  $N$ -body simulations are accurate, even though individual simulations are not (see, e.g., Boekholt & Portegies Zwart 2015).

## 5. Pre-impact orbit

Using  $t_{\text{impact}}$ ,  $\lambda_{\text{impact}}$ , and  $\phi_{\text{impact}}$  to select the best solution and after a few million trials, we obtain the orbital solution (see Tables 1 and 2):  $a = 1.62470348$  AU,  $e = 0.53184268$ ,  $i = 3^\circ.9749908$ ,  $\Omega = 326^\circ.4607324$ ,  $\omega = 109^\circ.7012184$ , and  $\tau = 2456292.5834112$  JDCT, with a value of the geocentric velocity at impact of  $17.74 \text{ km s}^{-1}$  and an impact probability  $>0.99999$ . The value of the velocity derived by Miller et al. (2013) from satellite data and video recordings amounts to  $17.7 \pm 0.5 \text{ km s}^{-1}$ . A value of  $17.6 \text{ km s}^{-1}$  is also favored in Proud (2013). The agreement between our virtual impact parameter results and the observational values, both in terms of impact time and coordinates, is very good (see Table 2 and Figure 6). The velocity at  $h_{\text{impact}}$  also matches well the one derived by Miller et al. (2013). Therefore, it is a reasonable solution—statistically speaking—to the inverse problem pointed out above. This new, most probable orbital solution is not too different from that in Paper II and matches well the one originally computed by S. Nakano (see Table 1 in Paper II).<sup>5</sup>

A problematic issue that compromises the uniqueness of any impact solution is in the uncertainty associated with the value of the geocentric velocity at  $h_{\text{impact}}$ . Proud (2013) already pointed out a range of  $17\text{--}18.6 \text{ km s}^{-1}$  in  $v_{\text{impact}}$ , generating extreme minimum and maximum trajectories. The U.S. Government sensors give a value of  $18.6 \text{ km s}^{-1}$  (no errors quoted) for the pre-impact geocentric velocity at an altitude of  $23.3 \text{ km}$  (peak brightness); the value has been obtained by D. Yeomans and P. Chodas.<sup>12</sup> Table S1 in Popova et al. (2013) shows that the value of the apparent velocity of the superbolide remained fairly constant between the altitudes of  $97.1$  and  $27 \text{ km}$ . On the other hand, in Table 1 of Borovička et al. (2013) it is indicated that the speed of the Chelyabinsk impactor relative to the Earth’s surface high in the atmosphere was  $19.03 \pm 0.13 \text{ km s}^{-1}$ ; the value of the apparent velocity at the entry point ( $97.1 \pm 1.6 \text{ km}$  above the ground) of the Chelyabinsk meteoroid given in Table S1 of Popova et al. (2013) is  $19.16 \pm 0.15 \text{ km s}^{-1}$ . The values of the velocities obtained from our simulations are true geocentric values rather than apparent ones as like those quoted in some of the papers cited. But what is the effect of the uncertainty in  $v_{\text{impact}}$  on the orbital solution?

In an attempt to answer the legitimate concern that prompted this question, we have performed additional calculations using the same data in terms of impact time and coordinates, but changing the model so suitable values of  $v_{\text{impact}}$  are obtained. We have used the same approach described above but this time forcing the model (the orbital parameters) to reach values of  $v_{\text{impact}}$  equal to  $\sim 17 \text{ km s}^{-1}$  (SOL0, left-hand column in Table 3),  $\sim 18.6 \text{ km s}^{-1}$  (SOL2, center column in Table 3),

---

<sup>12</sup><http://neo.jpl.nasa.gov/fireball/>

Table 2: Heliocentric Keplerian Orbital Elements of the Chelyabinsk Impactor at Epoch JDCT 2456337.63888889 from our  $N$ -body Approach

Semimajor axis, $a$ (AU)	$1.62470348 \pm 0.00000005$
Eccentricity, $e$	$0.53184268 \pm 0.00000002$
Inclination, $i$ (deg)	$3.9749908 \pm 0.0000008$
Longitude of the ascending node, $\Omega$ (deg)	$326.4607324 \pm 0.0000014$
Argument of perihelion, $\omega$ (deg)	$109.7012184 \pm 0.0000008$
Mean anomaly, $M$ (deg)	$21.4432449 \pm 0.0000013$
Time of perihelion passage, $\tau$ (JDCT)	$2456292.5834112 \pm 0.0000010$
	2012 Dec 31 02:00:06.6 UT
Perihelion, $q$ (AU)	$0.760616827 \pm 0.000000012$
Aphelion, $Q$ (AU)	$2.48879014 \pm 0.00000010$
Impact time, $t_{\text{impact}}$ (JDCT)	$2456338.6391296 \pm 0.0000009$
	2013 Feb 15 03:20:20.8 UT
Longitude of impact, $\lambda_{\text{impact}}$ (deg)	$64.5649 \pm 0.0014$
Latitude of impact, $\phi_{\text{impact}}$ (deg)	$+54.4450 \pm 0.0007$
Altitude of impact, $h_{\text{impact}}$ (km)	$97.9 \pm 0.3$
Velocity at impact, $v_{\text{impact}}$ (km s $^{-1}$ )	$17.74110 \pm 0.00013$
Radiant R.A., $\alpha_0$ (deg)	$334.23104 \pm 0.00005$
Radiant decl., $\delta_0$ (deg)	$-0.14575 \pm 0.00005$
Radiant velocity, $v_g$ (km s $^{-1}$ )	$13.86900 \pm 0.00005$

Note. Values include the  $1\sigma$  uncertainty. These values are the result of the average of the 36 best solutions ranked as explained in the text. The impact probability associated with this solution is  $>0.99999$ . The values of the velocities quoted here are geocentric and not apparent. In the following this is considered as SOL1.

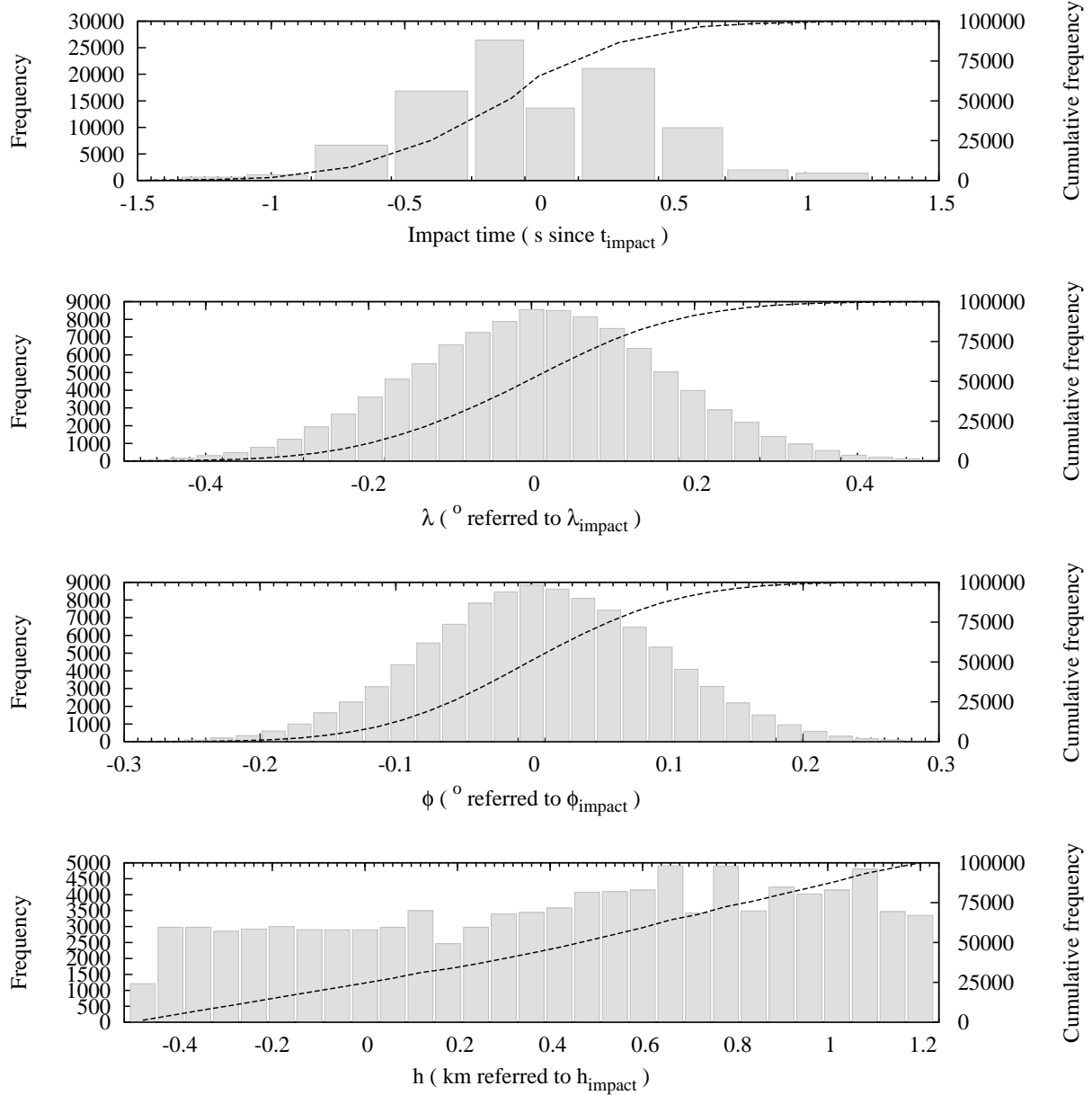


Fig. 6.— Resulting distribution in impact parameter space ( $t$ ,  $\lambda$ ,  $\phi$ , and  $h$ ) for an experiment using the orbital solution in Table 2 and  $10^5$  test orbits. The setup is equivalent to those of Figures 3–5. The values of the virtual impact parameters are referred to those in Popova et al. (2013) as pointed out above. The rather ragged distribution in impact time is the result of the unavoidable discretization of the output interval that also has an effect on the distribution in altitude.

and  $\sim 19.1 \text{ km s}^{-1}$  (SOL3, right-hand column in Table 3). The impact probabilities associated with these orbital solutions are all  $> 0.99999$ . If we compare the orbital solutions in Table 1 with those in Table 3 it is easy to realize why some of the published solutions fail to generate any significant impacts. If  $v_{\text{impact}}$  was  $\sim 19.1 \text{ km s}^{-1}$  then the closest solution (but still far from satisfactory, see above) is the one in Emel’Yanenko et al. (2014).

As in the case of SOL1, the agreement between our virtual impact parameter results and the observational values, both in terms of impact time and coordinates, is very good and their impact probabilities essentially equal to 1. However, the  $v_{\text{impact}}$  and the parameters of the true radiant (see below) of these alternative solutions are quite different. Fortunately, the orbital elements follow a linear relationship with  $v_{\text{impact}}$  and if a truly robust value of this parameter is eventually found (for example, from still unreleased military radar data), the following equations can be used to determine a first approximation for the appropriate orbit ( $a$  in AU,  $i$ ,  $\Omega$ , and  $\omega$  in degrees,  $\tau$  in JDCT, and  $v_{\text{impact}}$  in  $\text{km s}^{-1}$ ):

$$a = (0.144 \pm 0.005) v_{\text{impact}} - (0.93 \pm 0.09), r^2 = 0.9979, \quad (2)$$

$$e = (0.0476 \pm 0.0005) v_{\text{impact}} - (0.313 \pm 0.009), r^2 = 0.9998, \quad (3)$$

$$i = (0.86 \pm 0.03) v_{\text{impact}} - (11.3 \pm 0.6), r^2 = 0.9970, \quad (4)$$

$$\Omega = (-0.0082 \pm 0.0005) v_{\text{impact}} + (326.606 \pm 0.008), r^2 = 0.9935, \quad (5)$$

$$\omega = (-0.342 \pm 0.011) v_{\text{impact}} + (115.8 \pm 0.2), r^2 = 0.9978, \quad (6)$$

$$\tau = (1.17 \pm 0.03) v_{\text{impact}} + (2456271.8 \pm 0.5), r^2 = 0.9989, \quad (7)$$

These expressions have been obtained from SOL0 to SOL3 and their correlation coefficients, or Pearson’s  $r$  (see, e.g., Press et al. 2007), are very good. However, the precision of the values obtained from these equations is limited by the errors associated with the linear regression parameters (one to three decimal places, depending on the orbital element). These expressions give relatively low-precision estimates for the values of the orbital elements and may not apply outside the  $v_{\text{impact}}$  range of (17, 19.1)  $\text{km s}^{-1}$ .

Table 3: Alternative Heliocentric Keplerian Orbital Elements of the Chelyabinsk Impactor at Epoch JDCT 2456337.63888889 from our  $N$ -body Approach.

Semimajor axis, $a$ (AU)	1.53892950±0.00000004	1.74875174±0.00000003	1.83680075±0.00000005
Eccentricity, $e$	0.49874206±0.00000002	0.572221340±0.000000009	0.596987671±0.000000015
Inclination, $i$ (deg)	3.4927759±0.00000005	4.7550334±0.00000005	5.2563565±0.00000007
Longitude of the ascending node, $\Omega$ (deg)	326.4672008±0.00000008	326.4537788±0.00000007	326.4504518±0.00000010
Argument of perihelion, $\omega$ (deg)	109.9462609±0.00000009	109.4416222±0.00000005	109.2257672±0.00000007
Mean anomaly, $M$ (deg)	23.6960400±0.00000013	18.7763467±0.00000006	17.2169040±0.00000009
Time of perihelion passage, $\tau$ (JDCT)	2456291.7402523±0.00000007	2456293.5834773±0.00000004	2456294.1534305±0.00000006
	2012 Dec 30 05:45:57.8 UT	2013 Jan 01 02:00:12.4 UT	2013 Jan 01 15:40:56.4 UT
Perihelion, $q$ (AU)	0.771400634±0.000000012	0.748078675±0.000000010	0.740253347±0.000000012
Aphelion, $Q$ (AU)	2.30645836±0.00000008	2.74942480±0.00000006	2.93334814±0.00000011
Impact time, $t_{\text{impact}}$ (JDCT)	2456338.6391287±0.00000005	2456338.6391305±0.00000005	2456338.6391287±0.00000005
	2013 Feb 15 03:20:20.7 UT	2013 Feb 15 03:20:20.9 UT	2013 Feb 15 03:20:20.7 UT
Longitude of impact, $\lambda_{\text{impact}}$ (deg)	64.566±0.008	64.567±0.008	64.567±0.009
Latitude of impact, $\phi_{\text{impact}}$ (deg)	+54.441±0.004	+54.447±0.005	+54.443±0.005
Altitude of impact, $h_{\text{impact}}$ (km)	96.87±0.11	98.16±0.13	96.8±0.2
Velocity at impact, $v_{\text{impact}}$ (km s <sup>-1</sup> )	17.06933±0.00007	18.59238±0.00007	19.13400±0.00010
Radiant R.A., $\alpha_0$ (deg)	334.58835±0.00005	333.65322±0.00004	333.26714±0.00004
Radiant decl., $\delta_0$ (deg)	-0.65857±0.00005	+0.786599±0.000009	+1.31902±0.00004
Radiant velocity, $v_g$ (km s <sup>-1</sup> )	12.99800±0.00005	14.94270±0.00005	15.61070±0.00005

Note. Values include the  $1\sigma$  uncertainty. The impact probabilities associated with these solutions are >0.99999. The values of the velocities quoted here are geocentric and not apparent. In the following these solutions are referred to as SOL0 (left-hand column), SOL2 (center column), and SOL3 (right-hand column).

Another important observational parameter associated with an impact event is the radiant or point in the sky from which the incoming meteor appeared to originate. Figure 7, top panel, shows the location in geocentric equatorial coordinates of the radiant point as initially computed by Borovička et al. in CBET 3423 (Green 2013; gray point and error bars), Borovička et al. (2013; black point and error bars), and Popova et al. (2013; pink point and error bars). Aiming at comparing with these observational determinations, we have computed the true radiant geocentric equatorial coordinates associated with the orbital solution in Table 2. In order to understand better the effect of uncertainties in the computation of both radiants and impact points we have performed three sets of simulations with  $2 \times 10^4$  test orbits each: the first set has been generated within  $1\sigma$  of the values in Table 2, the second set corresponds to a  $10\sigma$  spread, and the third one has a  $100\sigma$  dispersion. The test orbits have been computed using uniformly distributed random numbers—not Gaussian like in the rest of this work—in order to survey the relevant volume of the orbital parameter space evenly. The geocentric equatorial coordinates resulting from our simulations are true values. In contrast, observational determinations give us the position of the incoming object when its light left the impactor. These apparent values have to be corrected for this time delay to obtain the true position of the object in the sky when it was observed. No comments are made in Green (2013), Borovička et al. (2013), or Popova et al. (2013) regarding possible corrections; however, the error bars in Green (2013) or Popova et al. (2013) are so large that any correction made is probably irrelevant. The arc in coordinates of the geocentric radiant described by SOL0 to SOL3 goes from  $(22^{\text{h}}306, -0^{\circ}659)$  to  $(22^{\text{h}}218, +1^{\circ}319)$  and its geocentric velocity,  $v_g$ , ranges from 12.998 to 15.611  $\text{km s}^{-1}$ . The value of  $v_g$  in Borovička et al. (2013) is  $15.14 \pm 0.16 \text{ km s}^{-1}$ ; Popova et al. (2013) gives a value of  $15.3 \pm 0.4 \text{ km s}^{-1}$ . The approximate values of the coordinates of the geocentric radiant,  $\alpha_0$  and  $\delta_0$ , and  $v_g$ , as a function of  $v_{\text{impact}}$  for solutions SOL0 to SOL3 are given by the expressions ( $\alpha_0$  and  $\delta_0$  in degrees, and  $v_g$  and  $v_{\text{impact}}$  in  $\text{km s}^{-1}$ ):

$$\alpha_0 = (-0.64 \pm 0.03) v_{\text{impact}} + (345.6 \pm 0.5), r^2 = 0.9965, \quad (8)$$

$$\delta_0 = (0.98 \pm 0.05) v_{\text{impact}} - (17.4 \pm 0.9), r^2 = 0.9953, \quad (9)$$

$$v_g = (1.265 \pm 0.009) v_{\text{impact}} - (8.6 \pm 0.2), r^2 = 0.9999. \quad (10)$$

The colored spot in Figure 7, top panel, shows the true position of the radiant associated with the orbital solution in Table 2 (SOL1). A magnified version of that area is displayed in the middle panel of Figure 7. Here, the panel shows the true geocentric equatorial coordinates of the virtual impactors at the beginning of the simulation, i.e., at epoch 2456337.63888889 JDCT. The points in red correspond to the set of test orbits with orbital elements within  $1\sigma$  of the solution in Table 2, those in blue have a  $10\sigma$  spread, and the green ones have  $100\sigma$ . Each virtual impactor generates one point on the bottom panel of Figure 7 following the same color pattern. The distribution on the surface of the Earth of the virtual impacts studied in Figure 7 is better visualized in Figure 8 where the virtual impacts define an arc extending from the Black Sea to the Siberian Plain if deviations as high as  $100\sigma$  are allowed in the initial conditions. The separation in impact time between the two most extreme test orbits in the  $100\sigma$  set is nearly 3.5 minutes. The projected flight path of the nominal solution in Table 2 is plotted as a red curve. This figure is similar to

panel (b), Figure 5 in Sitarski (1998). Figure 7, bottom panel, gives a very clear idea of how precise an orbital solution must be in order to make reliable predictions regarding the location of a future strike once a candidate impactor has been identified. The direction of flight in Figure 8 matches well that in Figure 4 in Miller et al. (2013). Figure 9 shows a comparison between our results and those shown in Figure 5 in Miller et al. (2013). The satellite-derived (blue) and surface-based video (red) reconstructions of the impact trajectory of the Chelyabinsk superbolide presented by Miller et al. (2013) are part of the  $3\sigma$  sample associated with the solution in Table 2.

The values of the coordinates of the geocentric radiant are  $\alpha_0 = 334^\circ 23' 10.4 \pm 0^\circ 00' 00.5$  (or  $22^{\text{h}} 28' 20.69 \pm 0^{\text{h}} 00' 00.03$ ) and  $\delta_0 = -0^\circ 14' 57.5 \pm 0^\circ 00' 00.5$ ; the geocentric velocity associated with the radiant is  $v_g = 13.86900 \pm 0.00005 \text{ km s}^{-1}$ . Apparently, there is a documented meteor stream that may be associated with this radiant. Terentjeva & Bakanas (2013) have pointed out that the Daytime Pegasids-Aquariids could be the source of the Chelyabinsk impactor. The parameters in their Table 1 marginally match those in our Table 2 although no estimates of the values of the errors are given in their work. This meteor shower is not documented in the extensive list compiled by Jenniskens (2006), however. Given the tentative link pointed out in Paper II between Chelyabinsk and other LL5 chondrite falls (see Section 5 in Paper II), this finding just adds another piece to this fascinating puzzle.

## 6. Related objects and dynamical evolution

The cosmic-ray exposure age of the Chelyabinsk meteoritic samples has been determined to be about 1.2 Myr (see, e.g., Popova et al. 2013). This relatively young age can be interpreted as the approximate time elapsed since the surface of the impactor was first exposed to cosmic rays, probably as a result of a break-up event. Figure 10 shows the results of the backwards integration of eleven control orbits plus the nominal one in an attempt to explore the probable location of the Chelyabinsk asteroid 1.2 Myr ago, according to the orbital solution in Table 2. Our full  $N$ -body reconstruction of the pre-impact orbit of the Chelyabinsk impactor in Figure 10 places this object directly in the region from 1.2 to 2.8 AU at that time. About 36% of the orbits have values of the semimajor axis below that of Mars. Another 36% have  $a$  around 1.7 AU. The rest are trapped inside the secular resonance  $\nu_6$  and jumping into the strong 4:1 mean motion resonance with Jupiter at 2.064 AU as described in Scholl & Froeschlé (1991) or even at the 3:1 orbital resonance with Jupiter (at 2.5 AU) as described by, e.g., Gladman et al. (1997). The figure also shows that the control orbits experience multiple episodes of horizontal (resonant) oscillations. In any case, and if the Chelyabinsk impactor was formed during a fragmentation event nearly 1.2 Myr ago, it is virtually impossible that any related fragments could still be moving in orbits very similar to that in Table 2. However, if the path followed by the impactor during the last 1 Myr or so is regarded as a delivery route as described in Morbidelli et al. (1994), it is perfectly possible that other, physically unrelated minor bodies could be following orbits similar to that of the Chelyabinsk impactor, forming a dynamical or resonant group.

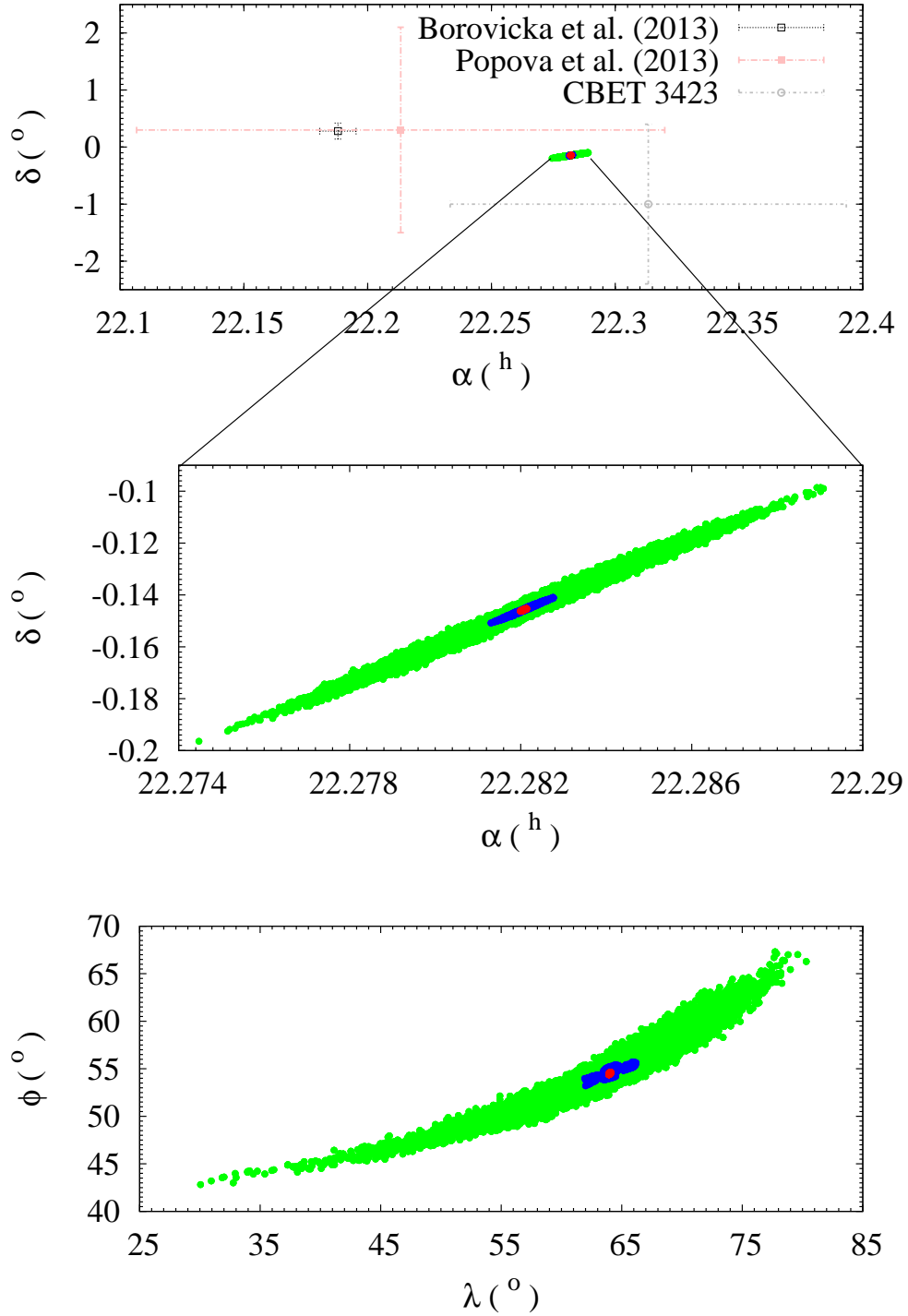


Fig. 7.— Geocentric equatorial coordinates of the radiant (top and middle panels) and their associated virtual impact coordinates (bottom panel). Virtual impacts plotted in green represent those associated with sets of orbital elements within  $100\sigma$  of those in Table 2, the ones in blue are the result of a  $10\sigma$  spread, and those in red are restricted to  $1\sigma$  (see the text for further details).

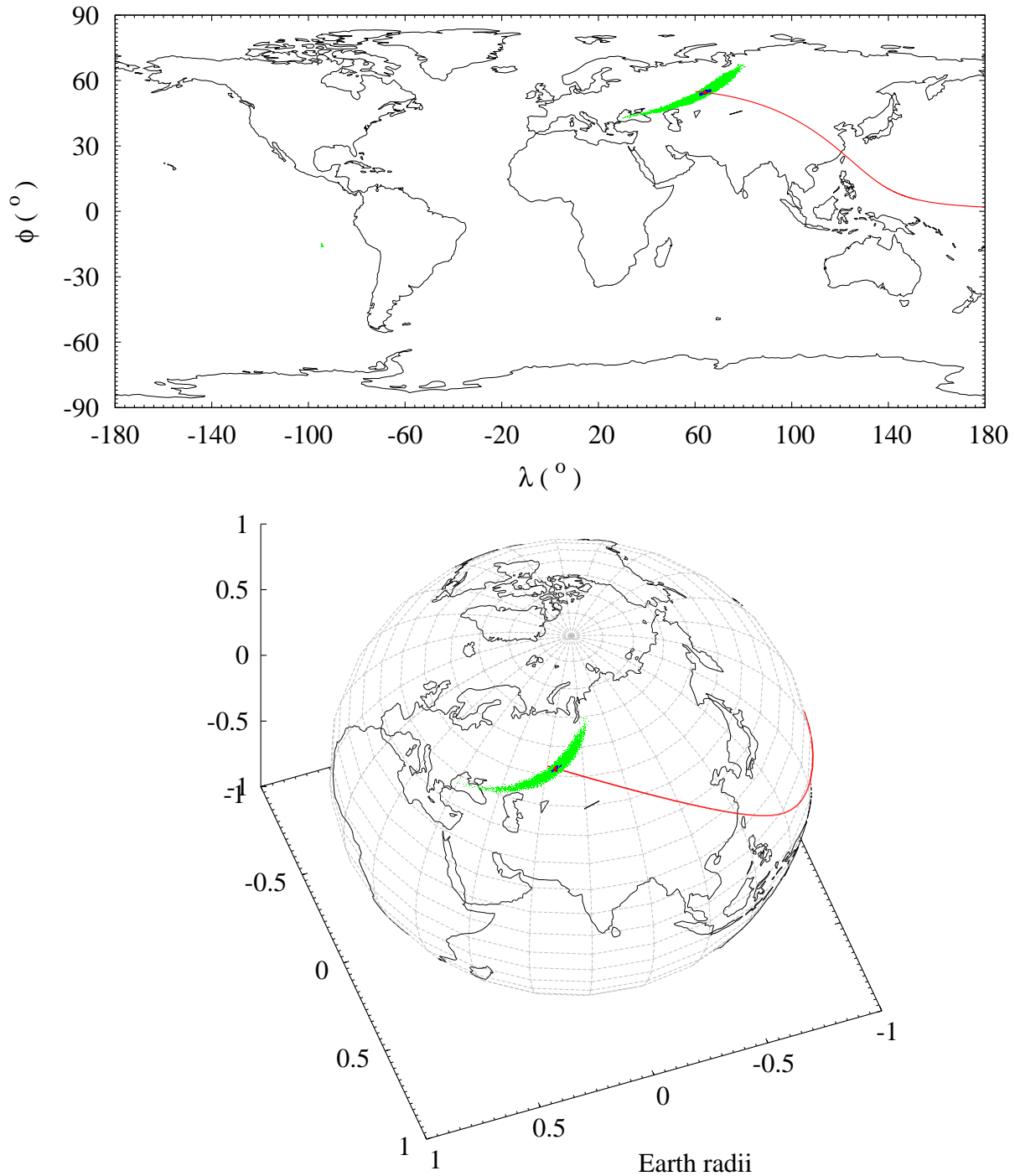


Fig. 8.— Distribution on the surface of the Earth of the virtual impacts studied in Figure 7, using the same color coding. The virtual impacts define an arc extending from the Black Sea to the Siberian Plain if deviations as high as  $100\sigma$  are considered. The projected flight path of the nominal solution in Table 2 is plotted as a red curve.

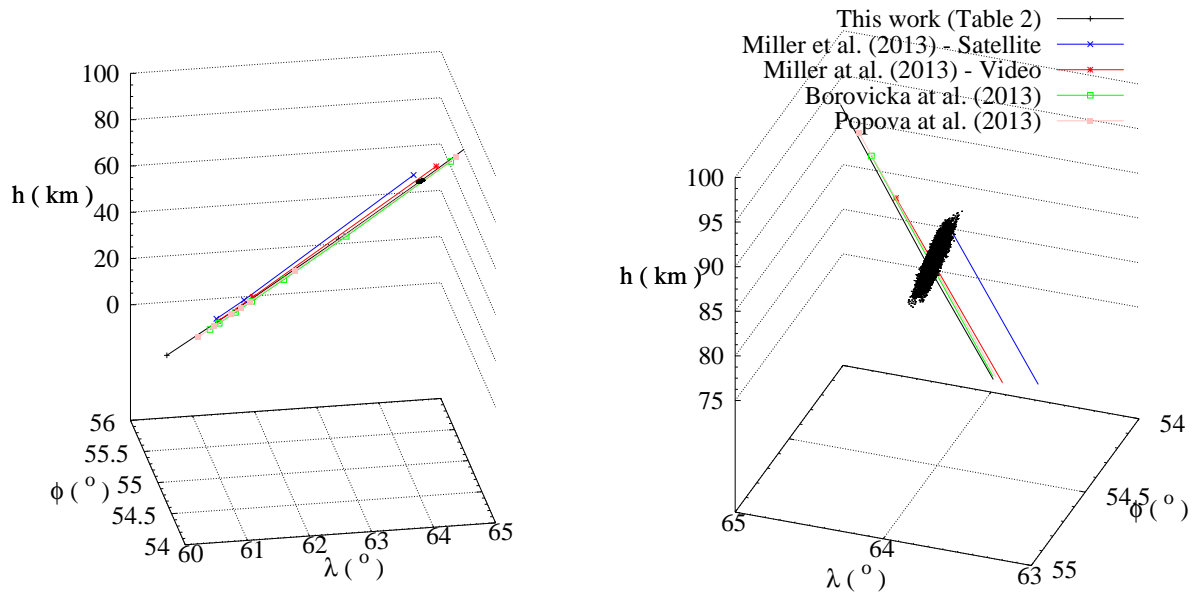


Fig. 9.— Terminal phase of the impact trajectory of the Chelyabinsk superbolide as described by the solution in Table 2, the two determinations shown in Figure 5 in Miller et al. (2013), and those in Table 1 in Borovička et al. (2013) and Table S1 in Popova et al. (2013). The virtual impacts plotted as red points in Figures 7 and 8 are replotted here as black dots. The right-hand figure is a rotated and magnified version of the left-hand figure.

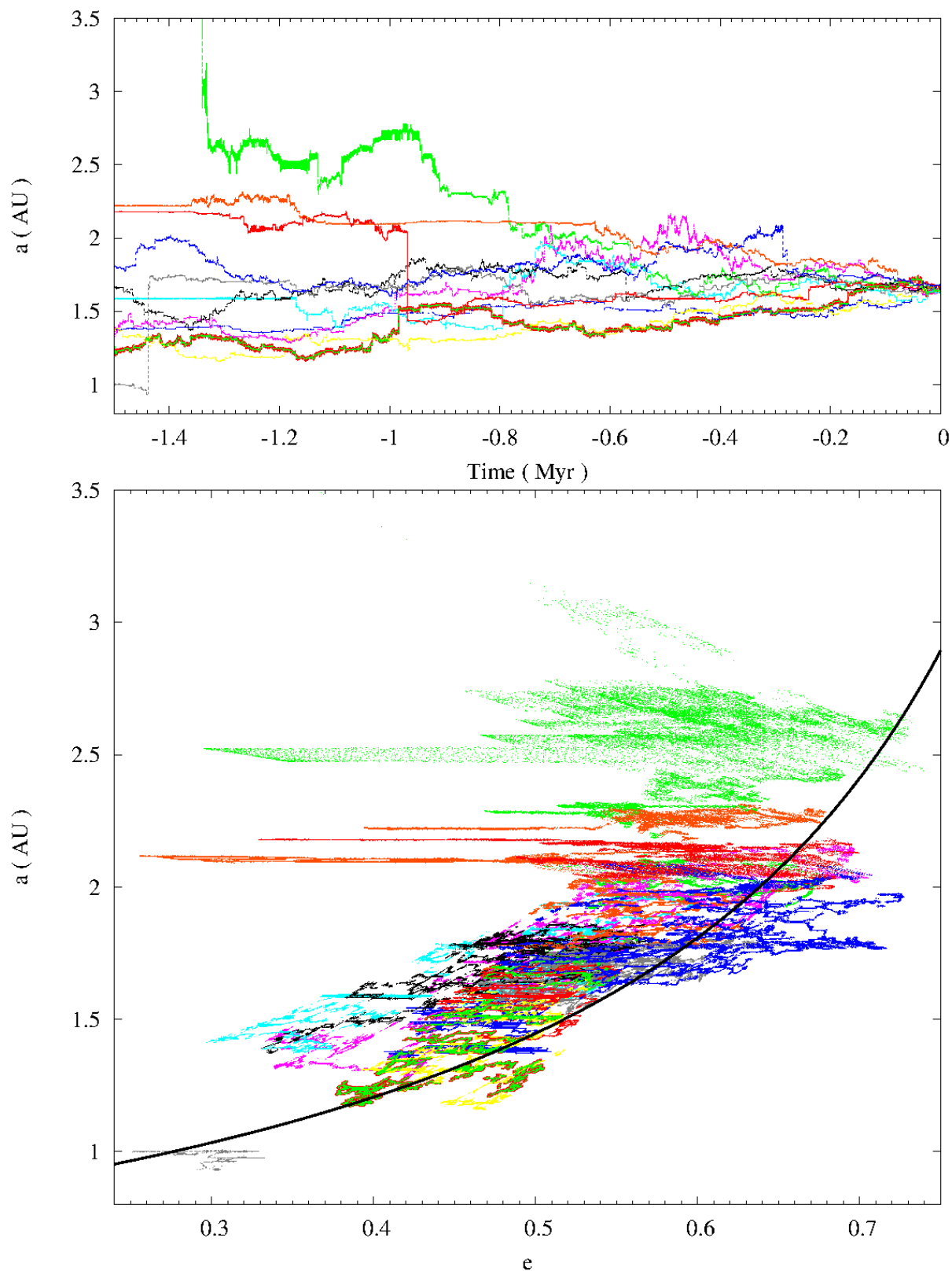


Fig. 10.— Time evolution of the orbital element  $a$  of multiple control orbits of the Chelyabinsk impactor as described by the solution displayed in Tables 1 and 2 (top panel), and evolution of the same orbits in the  $e$ - $a$  plane (bottom panel). Eleven control orbits are plotted; the nominal one is the thick red/green curve. The continuous line represents the  $(e, a)$  combination with perihelion

Assuming that other objects could be moving in similar orbits, we use the  $D$ -criteria of Southworth & Hawkins (1963,  $D_{\text{SH}}$ ), Lindblad & Southworth (1971,  $D_{\text{LS}}$ ), Drummond (1981,  $D_{\text{D}}$ ), and the  $D_{\text{R}}$  from Valsecchi et al. (1999) to investigate possible dynamical connections between this object and known minor bodies. A search among all the objects currently catalogued (as of 2015 August 19) by the JPL Small-Body Database<sup>13</sup> using these criteria gives the list of candidates in Table 4. With a few exceptions, their orbits are poorly constrained as they are based on short arcs but they are provided here to encourage further observations. All of them are classified as Apollos, near-Earth asteroids (NEAs) and, a few, as potentially hazardous asteroids (PHAs); their aphelia are in or near the 3:1 orbital resonance with Jupiter (at 2.5 AU). These objects are strongly perturbed as they experience periodic close encounters not only with the Earth–Moon system but also with Mars, Ceres and, in some cases, Venus. They are also subjected to multiple secular resonances (see Paper II). Figure 11 compares the evolution of the orbital parameters of the Chelyabinsk impactor as described by the solution displayed in Tables 1 and 2 and 2011 EO<sub>40</sub> that is the known NEO with the lowest values of the various  $D$ -criteria. Also plotted is the evolution of 2003 BR<sub>47</sub>, which is the object (also NEO and PHA like 2011 EO<sub>40</sub>) with the closest orbit to that of the impactor—as characterized in Table 2—if the five orbital elements are considered ( $a = 1.6283325$  AU,  $e = 0.5001041$ ,  $i = 4^\circ 42' 08''$ ,  $\Omega = 314^\circ 56' 87.5''$ , and  $\omega = 112^\circ 52' 03.8''$ , nominal precision with  $D_{\text{SH}} = 0.1037$ ,  $D_{\text{LS}} = 0.0626$ ,  $D_{\text{D}} = 0.0529$ , and  $D_{\text{R}} = 0.0948$ ). Data in Figure 11 are the result of averaging 100 control orbits generated after applying a Monte Carlo approach within the orbital parameter domain limited by the available  $1\sigma$  uncertainties (see Table 5) and using Gaussian random numbers. The average time evolution of the various  $D$ -criteria for 2003 BR<sub>47</sub> and 2011 EO<sub>40</sub> is displayed in Figure 12; this comparison is customarily used to link meteors and NEOs (see, e.g., Trigo-Rodríguez et al. 2007; Olech et al. 2015). Statistically speaking, the Chelyabinsk impactor is a robust dynamical relative of 2011 EO<sub>40</sub> as described by SOL1: the ranges of their orbital parameters,  $a$ ,  $e$ , and  $i$ , fully overlap after about 100 years of backwards integration. Candidate dynamical relatives for SOL0, SOL2, and SOL3 are compiled in Tables 6–8, respectively.

---

<sup>13</sup><http://ssd.jpl.nasa.gov/sbdb.cgi>

Table 4: Orbital Elements, Orbital Periods ( $P_{\text{orb}}$ ), Perihelia ( $q = a(1 - e)$ ), Aphelia ( $Q = a(1 + e)$ ), Number of Observations ( $n$ ), Data arc, and Absolute Magnitudes ( $H$ ) of Objects Moving in Orbits Similar to that of the Meteoroid that Caused the Chelyabinsk Superbolide as Described by the Solution Displayed in Tables 1 and 2

Asteroid	Epoch	$a$ (AU)	$e$	$i$ (deg)	$\Omega$ (deg)	$\omega$ (deg)	$P_{\text{orb}}$ (year)	$q$ (AU)	$Q$ (AU)	$n$	arc (d)	$H$ (mag)	$D_{\text{SH}}$	$D_{\text{LS}}$	$D_{\text{D}}$	$D_{\text{R}}$	PHA
2011 EO <sub>40</sub>	57000	1.6540887	0.54016233	3.36286	50.30284	17.07473	2.13	0.76	2.55	20	34	21.50	0.1198	0.0135	0.0396	0.0073	Yes
2002 AC <sub>9</sub>	57000	1.7038247	0.56051693	2.28428	2.58887	28.42304	2.22	0.75	2.66	51	3132	21.00	0.4232	0.0428	0.1407	0.0224	Yes
2014 SJ <sub>142</sub>	57000	1.5591764	0.50812802	2.08620	336.63875	119.15404	1.95	0.77	2.35	34	30	23.20	0.1821	0.0411	0.0623	0.0234	No
2012 QZ <sub>16</sub>	57000	1.5376728	0.50328326	6.11985	151.62956	258.93607	1.91	0.76	2.31	23	2	25.50	0.2902	0.0472	0.1007	0.0237	No
2015 CC <sub>1</sub>	57070	1.5467360	0.51434097	3.59953	88.60772	327.84872	1.92	0.75	2.34	22	16	23.88	0.2149	0.0209	0.0722	0.0248	No
2012 VA <sub>20</sub>	57000	1.6822360	0.55511183	4.39092	62.74253	240.11893	2.18	0.75	2.62	16	10	22.80	1.0048	0.0273	0.4053	0.0257	No
2013 BR <sub>15</sub>	56309	1.5546110	0.52043752	1.95468	102.89879	284.89340	1.94	0.75	2.36	10	2	25.00	0.4427	0.0400	0.1464	0.0260	No
2009 SD	55091	1.7343896	0.56682933	3.04789	344.32550	287.05721	2.28	0.75	2.72	24	3	25.40	1.0899	0.0397	0.5041	0.0265	No
1996 VB <sub>3</sub>	50401	1.6259062	0.54444404	2.79583	180.62271	132.68222	2.07	0.74	2.51	21	9	22.40	0.9520	0.0313	0.3687	0.0290	No
2014 AF <sub>5</sub>	57000	1.5671674	0.51925929	6.41394	100.65973	288.73045	1.96	0.75	2.38	24	1	28.80	0.4511	0.0450	0.1496	0.0301	No
2010 DU <sub>1</sub>	55247	1.6892222	0.54017890	3.70925	147.83081	74.25332	2.20	0.78	2.60	22	4	26.50	1.0339	0.0187	0.4344	0.0335	No
2013 UX	57000	1.6994971	0.56023315	5.44902	259.54850	51.72108	2.22	0.75	2.65	53	42	22.00	0.9724	0.0405	0.3799	0.0338	No
2015 AM <sub>45</sub>	57000	1.5512258	0.51739809	5.58246	275.22926	107.47502	1.93	0.75	2.35	46	48	22.10	0.4772	0.0338	0.1579	0.0344	No
2014 KW <sub>76</sub>	57000	1.6825498	0.56131222	2.33519	67.46190	102.00097	2.18	0.74	2.63	34	4	27.90	0.8000	0.0468	0.2857	0.0346	No
2004 RN <sub>251</sub>	57000	1.6558104	0.52789965	4.39200	179.60954	245.93613	2.13	0.78	2.53	27	2	26.10	0.1717	0.0227	0.0608	0.0360	No
2008 EF <sub>32</sub>	54536	1.6276459	0.52218191	1.73604	349.17686	112.26942	2.08	0.78	2.48	8	1	29.40	0.2353	0.0437	0.0767	0.0377	No
2007 BD <sub>7</sub>	57000	1.5624753	0.49802522	4.84926	343.62280	219.85002	1.95	0.78	2.34	185	14	21.10	0.9240	0.0440	0.3660	0.0385	Yes
2015 HR <sub>43</sub>	57000	1.5451866	0.51964396	4.59407	214.18500	274.35526	1.92	0.74	2.35	26	5	26.30	0.4821	0.0246	0.1605	0.0394	No
2011 GP <sub>28</sub>	57000	1.5046701	0.50455345	3.81544	16.27364	256.42378	1.85	0.75	2.26	14	1	29.40	1.0278	0.0313	0.4721	0.0406	No
2011 CZ <sub>3</sub>	57000	1.5971625	0.51105243	2.11411	326.23428	241.70050	2.02	0.78	2.41	30	4	26.30	0.9529	0.0436	0.3825	0.0426	No
2008 UT <sub>95</sub>	57000	1.8149119	0.57453004	3.81156	220.04223	247.43235	2.45	0.77	2.86	32	2	27.40	0.3219	0.0443	0.1115	0.0449	No
2014 OF <sub>392</sub>	56867	1.5128759	0.50967476	4.52466	117.73372	278.59135	1.86	0.74	2.28	12	5	25.50	0.3845	0.0306	0.1286	0.0451	No
2008 FH	54556	1.5849644	0.50476518	3.46186	5.20388	264.09916	2.00	0.78	2.38	25	12	24.30	1.0315	0.0375	0.4819	0.0453	No
1996 AW <sub>1</sub>	57000	1.5347586	0.51840437	4.75623	117.65829	229.26555	1.90	0.74	2.33	52	6975	19.80	0.7532	0.0288	0.2663	0.0458	Yes

Note. The various  $D$ -criteria ( $D_{\text{SH}}$ ,  $D_{\text{LS}}$ ,  $D_{\text{D}}$  and  $D_{\text{R}}$ ) are also shown. The objects are sorted by ascending  $D_{\text{R}}$ . Only objects with  $D_{\text{LS}} < 0.05$  and  $D_{\text{R}} < 0.05$  are shown. The epoch of the orbital elements is in Modified Julian Date (MJD), which is defined as the Julian date  $-2400000.5$ . Data as of 2015 August 19. Source: JPL Small-Body Database.

As pointed out above, it may be argued that studying the orbital evolution of a given minor planet by computing orbital elements of the control orbits and varying them randomly, within the ranges defined by their mean values and standard deviations, may lead to unphysical results. As a consistency test, we have used the MCCM approach to recompute the past orbital evolution of 2011 EO<sub>40</sub>, generating control orbits with initial parameters from the nominal orbit, adding random noise on each initial orbital element, and making use of the covariance matrix. A comparison between the results of the evolution of a sample of 100 control orbits generated using MCCM and the classical method for the particular case of 2011 EO<sub>40</sub> appears in Figure 13. These calculations show that, at least for this particular object, the difference is not very significant; our results are therefore robust. However, and for very precise orbits, the outcomes from these two approaches could be very different as we can clearly see in Figure 5 in Sitarski (1998) or in our analysis of the close encounter with 367943 Duende (2012 DA<sub>14</sub>) discussed above.

One may also be concerned about the possible influence of the Yarkovsky and Yarkovsky–O’Keefe–Radzievskii–Paddack (YORP) effects (see, e.g., Bottke et al. 2006) on our results. The largest predicted Yarkovsky drift rates are  $\sim 10^{-7}$  AU yr<sup>-1</sup> (see, e.g., Farnocchia et al. 2013), but the gravitationally induced changes in the values of the semimajor axes of 2003 BR<sub>47</sub>, 2011 EO<sub>40</sub>, and the virtual body associated with the solution displayed in Tables 1 and 2 are several orders of magnitude larger (see Figure 11). On the other hand, most asteroid fragments appear to be tumbling or in chaotic rotation, and the role of the Yarkovsky and YORP effects may be unimportant in these cases—but see the discussion in Vokrouhlický et al. (2015) for the particular case of 99942 Apophis (2004 MN<sub>4</sub>). Besides, accurate modeling of the Yarkovsky force requires relatively precise knowledge of the physical properties (for example, rotation rate, albedo, bulk density, surface conductivity, emissivity) of the objects involved, which is not the case here. The non-inclusion of these effects has no major impact on the assessment completed.

When we state that the Chelyabinsk impactor appears to be a robust dynamical relative of 2011 EO<sub>40</sub> we do not imply that they necessarily had a physical connection in the remote past or that they have followed similar orbits in the long term even if they are not genetically linked. We simply state that currently, and in the immediate past, both objects appear to have been subjected to the same average background perturbation, i.e., that they have been sharing (in relatively recent times) the same dynamical environment. In summary, they have been subjected to the same combination of secular resonances and cadence of close encounters with the objects pointed out above. Schunová et al. (2012) have shown that a robust statistical estimate of a dynamical relationship between objects that are part of the NEA population is only possible for groups of four or more objects. On the other hand, and owing to the dynamical issues described above, it is widely accepted that groups of objects moving initially in similar trajectories lose all orbital coherence in a short timescale (Pauls & Gladman 2005; Rubin & Matson 2008; Lai et al. 2014). Focusing on the NEO population, Schunová et al. (2012) could not find any statistically significant group of dynamically related objects among those currently known. However, Schunová et al. (2014) confirmed that streams from tidally disrupted objects can be detected for a few

Table 5: Heliocentric Keplerian Orbital Elements of 2003 BR<sub>47</sub> and 2011 EO<sub>40</sub> at Epoch JDCT 2457000.5 (2014 December 9.0)

	2003 BR <sub>47</sub>	2011 EO <sub>40</sub>
Semimajor axis, $a$ (AU)	$1.6283325 \pm 0.0000005$	$1.6541 \pm 0.0003$
Eccentricity, $e$	$0.5001041 \pm 0.0000006$	$0.54016 \pm 0.00011$
Inclination, $i$ (deg)	$4.42080 \pm 0.00002$	$3.3629 \pm 0.0007$
Longitude of the ascending node, $\Omega$ (deg)	$314.56875 \pm 0.00002$	$50.303 \pm 0.008$
Argument of perihelion, $\omega$ (deg)	$112.52038 \pm 0.00012$	$17.075 \pm 0.010$
Mean anomaly, $M$ (deg)	$274.3048 \pm 0.0009$	$312.6 \pm 0.2$
Perihelion, $q$ (AU)	$0.8139967 \pm 0.0000008$	$0.76061 \pm 0.00006$
Aphelion, $Q$ (AU)	$2.4426683 \pm 0.0000007$	$2.5476 \pm 0.0005$
Absolute magnitude, $H$ (mag)	21.4	21.5

Note. Values include the  $1\sigma$  uncertainty. Data as of 2015 August 19. Source: JPL Small-Body Database.

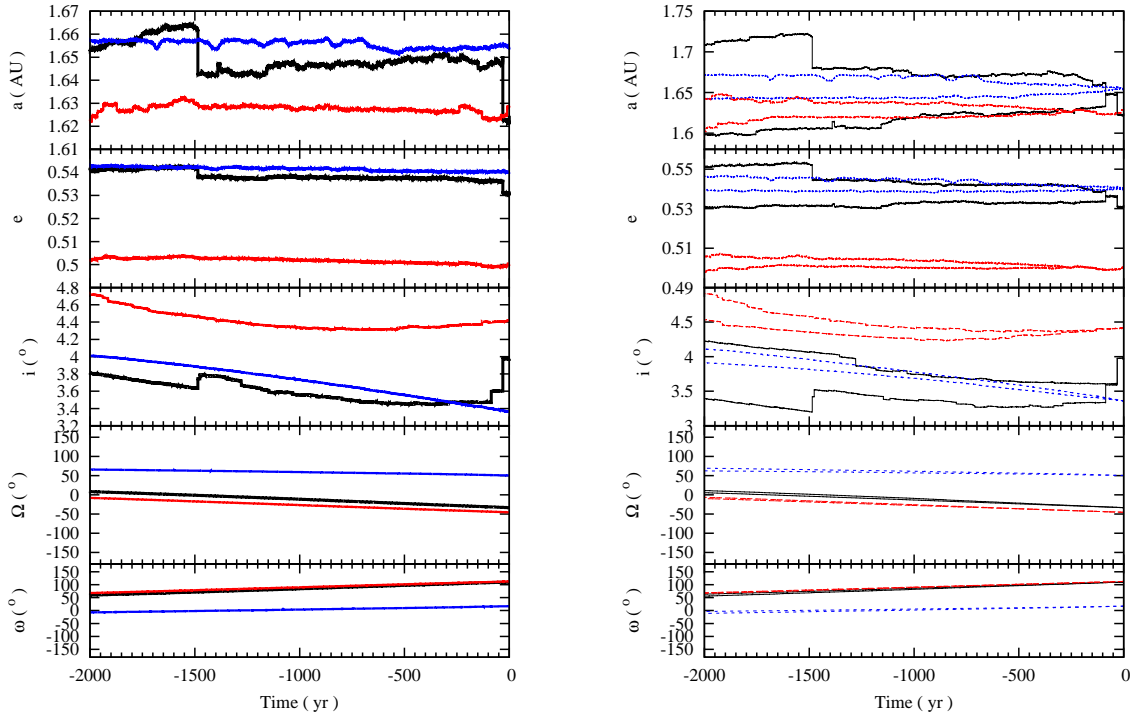


Fig. 11.— Time evolution of the orbital elements  $a$ ,  $e$ ,  $i$ ,  $\Omega$ , and  $\omega$  of 2003 BR<sub>47</sub> (red), 2011 EO<sub>40</sub> (blue), and the Chelyabinsk impactor (black) as described by the solution displayed in Tables 1 and 2. The left-hand panels show the average evolution of 100 control orbits, the right-hand panels show the ranges in the values of the parameters at the given time.

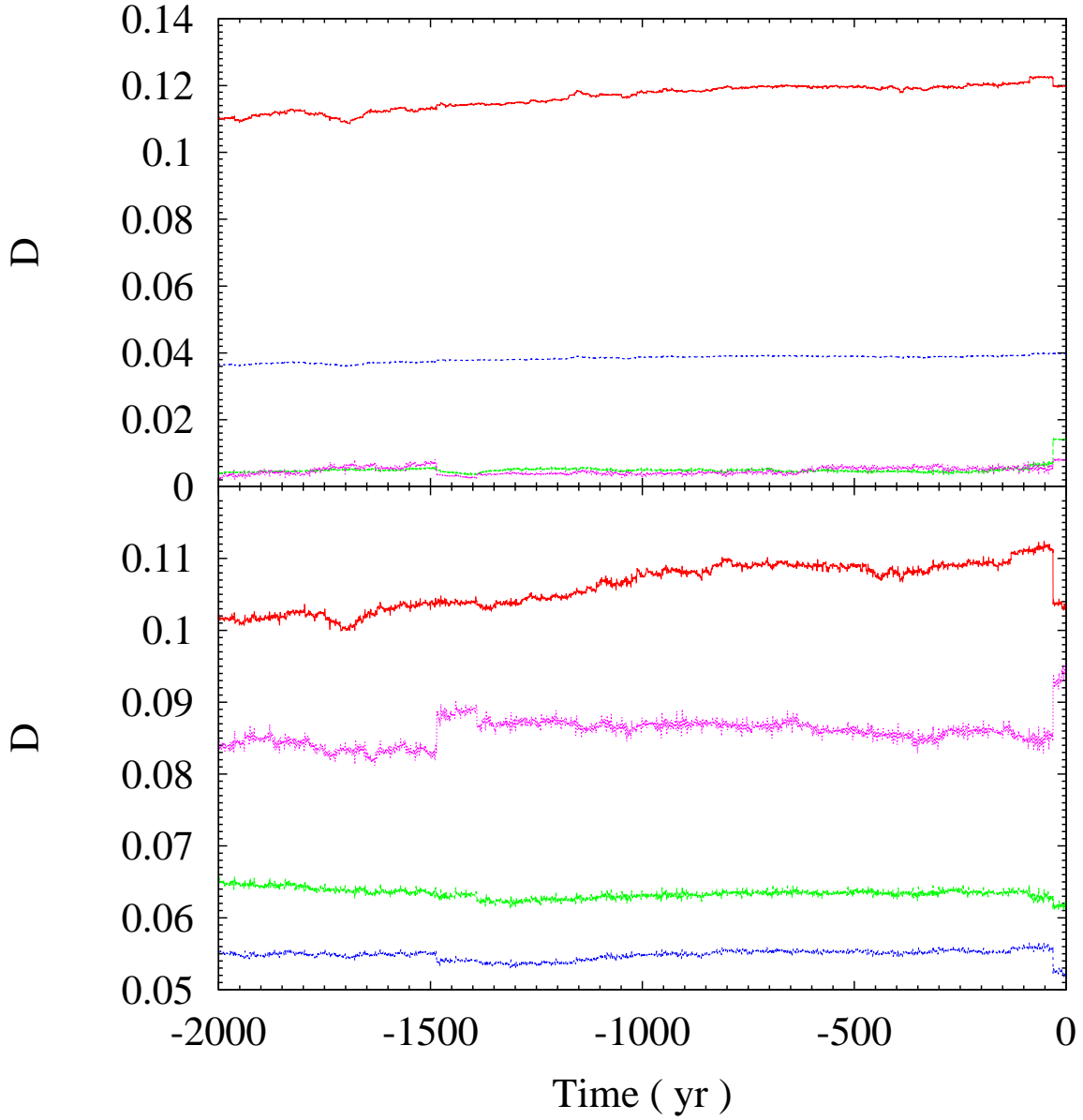


Fig. 12.— Average time evolution of the various  $D$ -criteria — $D_{\text{SH}}$  (red),  $D_{\text{LS}}$  (green),  $D_{\text{D}}$  (blue), and  $D_{\text{R}}$  (pink)— for 2011 EO<sub>40</sub> (top panel) and 2033 BR<sub>47</sub> (bottom panel) with respect to the Chelyabinsk impactor as described by the solution displayed in Tables 1 and 2. The values have been computed using the data in Figure 11, left-hand panels.

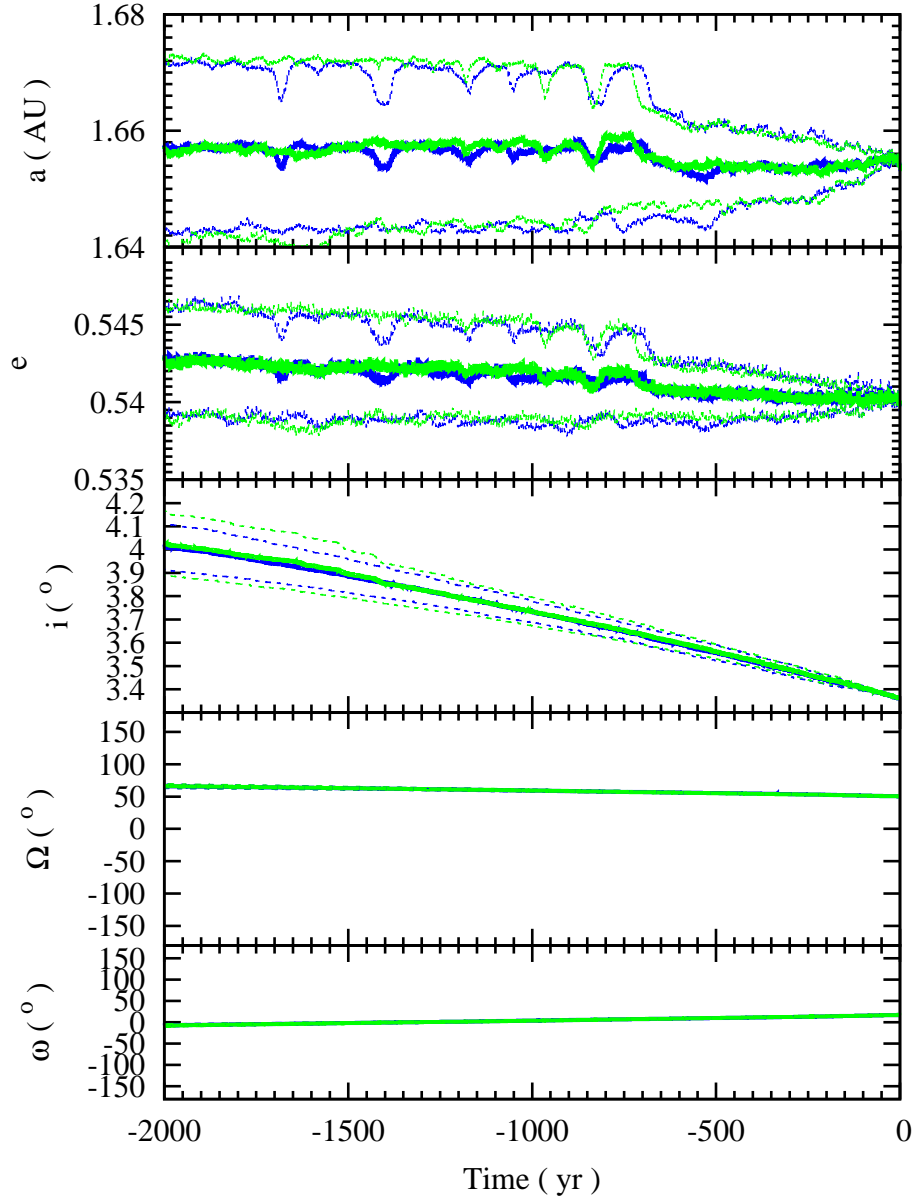


Fig. 13.— Time evolution of the orbital elements  $a$ ,  $e$ ,  $i$ ,  $\Omega$ , and  $\omega$  of 2011 EO<sub>40</sub>. In blue we replot the data in Figure 11; in green we show the results based on MCMC (see the text for details). In this figure both average values and their ranges are plotted. The magnitude of the deviations is comparable to that observed when integrations are carried out with a different number of perturbing asteroids.

thousand years after a hypothetical disruption event only if the parent body is large enough.

Returning to the topic of the most recent events in the dynamical history of the putative Chelyabinsk impactor as characterized by SOL1, all the simulations performed show that a few decades ago the object studied here suffered a dramatic change in its orbital elements  $a$ ,  $e$ , and  $i$ . Our calculations indicate that the Chelyabinsk impactor likely passed a gravitational keyhole (Chodas 1999) on 1982 February 15 ( $2445016.294 \pm 0.018$  JDCT, nominal uncertainty) during an encounter with our planet at  $d < 0.0015$  AU. As a result of this close encounter, its initial 2011 EO<sub>40</sub>-like trajectory was changed into the one that drove the meteoroid to strike the Earth nearly 31 years later (see Figure 14). Based solely on the number of computations performed, we estimate the likelihood of this event at  $>99.9\%$ . As the close approaches occurred at about the same time in different years, we can speak of a resonant return (Milani et al. 1999), thus the two orbits were nearly resonant as pointed out in Paper II. None of the other three solutions computed (SOL0, SOL2, or SOL3) traverses a gravitational keyhole of the strength of the one found for SOL1; in particular, the backwards evolution of SOL3 shows that it does not travel through any keyhole in the decades prior to its virtual impact. Only SOL1 produces a strong virtual resonant return. Asteroids 2011 EO<sub>40</sub> and 2003 BR<sub>47</sub> (and many others in Table 4) can undergo close encounters with Venus, our planet, and Mars but in general they are not synchronized or coupled in time with those of the Chelyabinsk impactor (SOL1). This fact suggests that any genetic connection between the impactor and these asteroids is unlikely, i.e., it cannot be a recent fragment of any of those minor bodies. However, and as we already pointed out in Paper II, 2011 EO<sub>40</sub> and the Chelyabinsk impactor (SOL1) tend to encounter the Earth at somewhat regular intervals (see Figure 15), but this could be mere coincidence.

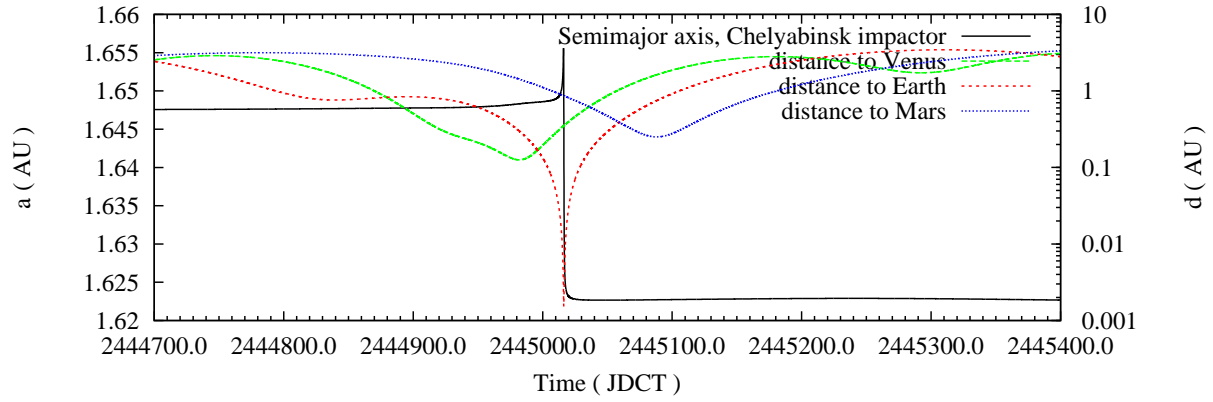


Fig. 14.— Time evolution of the orbital element  $a$  of the Chelyabinsk impactor (black) as described by the solution displayed in Tables 1 and 2, and the distances to Venus (green), the Earth (red), and Mars (blue) around the time (1982 February 15) the impactor passed a gravitational keyhole that led to the impact in 2013.

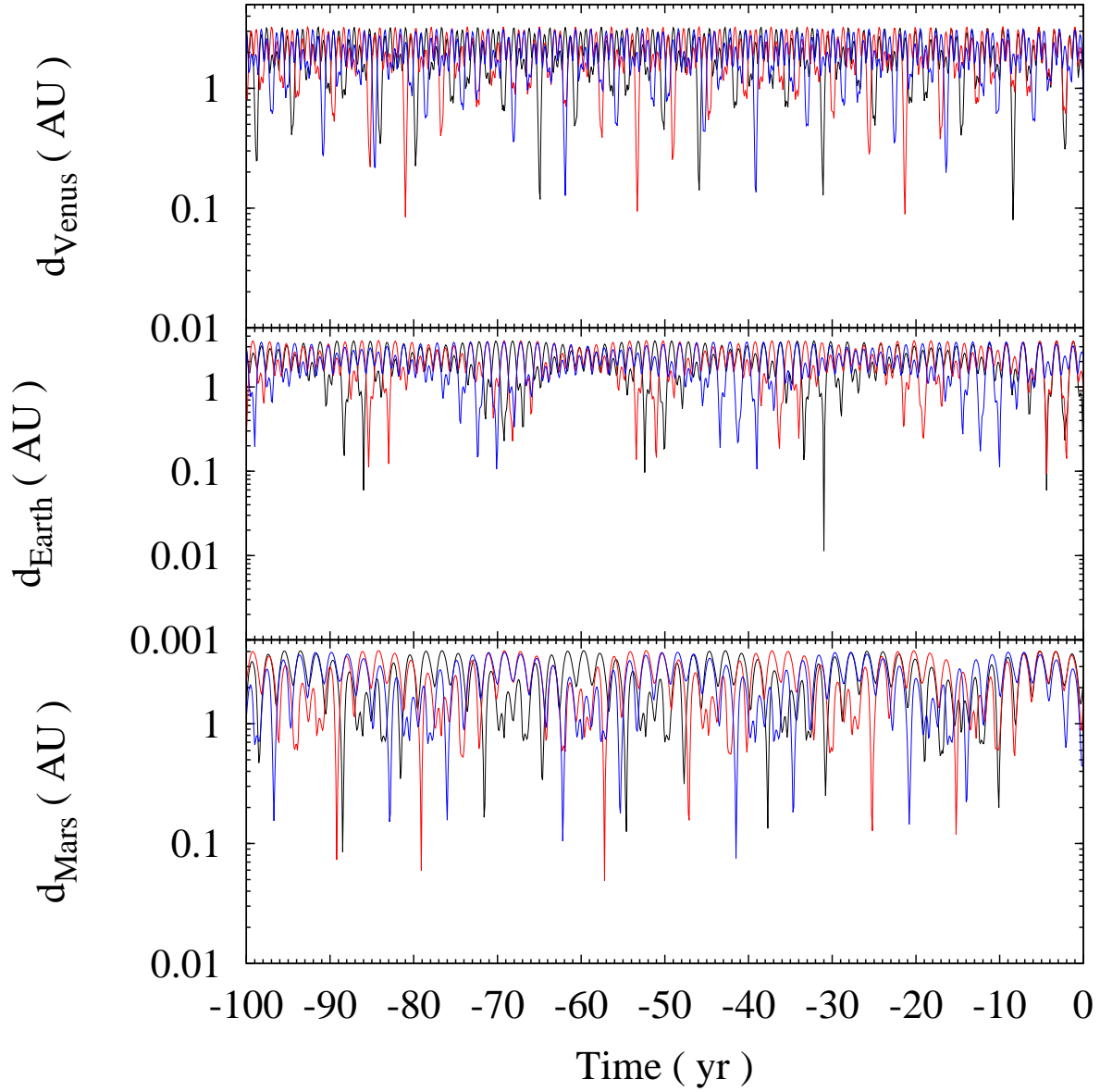


Fig. 15.— Distance from Venus (top panel), Earth (middle panel), and Mars (bottom panel) to the Chelyabinsk impactor (black) as described by the solution displayed in Tables 1 and 2, 2003 BR<sub>47</sub> (red), and 2011 EO<sub>40</sub> (blue). The data plotted here correspond to representative orbits from the sets displayed in Figure 11.

Table 6: Similar to Table 4 but for SOL0. Data as of 2015 August 19. Source: JPL Small-Body Database

Asteroid	Epoch	$a$ (AU)	$e$	$i$ (deg)	$\Omega$ (deg)	$\omega$ (deg)	$P_{\text{orb}}$ (year)	$q$ (AU)	$Q$ (AU)	$n$	arc (d)	$H$ (mag)	$D_{\text{SH}}$	$D_{\text{LS}}$	$D_{\text{D}}$	$D_{\text{R}}$	PHA
2004 RU <sub>109</sub>	57000	1.5324022	0.48927544	5.84931	171.40220	250.59089	1.90	0.78	2.28	50	1	26.40	0.2020	0.0437	0.0700	0.0059	No
2014 SJ <sub>142</sub>	57000	1.5591764	0.50812802	2.08620	336.63875	119.15404	1.95	0.77	2.35	34	30	23.20	0.1717	0.0267	0.0557	0.0061	No
2014 DA	57000	1.5055466	0.48456979	2.46494	313.70691	110.14161	1.85	0.78	2.24	142	21	22.70	0.1106	0.0233	0.0380	0.0145	No
2012 VQ <sub>6</sub>	56237	1.5074824	0.49522226	0.83915	211.51596	269.13667	1.85	0.76	2.25	29	5	27.00	0.3808	0.0476	0.1257	0.0147	No
2007 BD <sub>7</sub>	57000	1.5624753	0.49802522	4.84926	343.62280	219.85002	1.95	0.78	2.34	183	14	21.10	0.8928	0.0270	0.3519	0.0174	Yes
2011 EH	55622	1.4777343	0.48458290	2.34685	339.20374	96.57004	1.80	0.76	2.19	23	2	25.50	0.0292	0.0264	0.0176	0.0228	No
163679 (2002 XG <sub>84</sub> )	57000	1.4947103	0.47150532	5.05877	29.82729	349.62019	1.83	0.79	2.20	144	4729	19.20	0.4720	0.0428	0.1590	0.0258	No
2009 PQ <sub>1</sub>	57000	1.4971214	0.48930948	5.59308	326.94431	271.55318	1.83	0.76	2.23	81	29	22.50	0.9768	0.0385	0.4448	0.0267	No
2011 CZ <sub>3</sub>	57000	1.5971625	0.511105243	2.11411	326.23428	241.70050	2.02	0.78	2.41	30	4	26.30	0.9212	0.0287	0.3692	0.0277	No
2012 QZ <sub>16</sub>	57000	1.5376728	0.50328326	6.11985	151.62956	258.93607	1.91	0.76	2.31	23	2	25.50	0.2798	0.0467	0.0936	0.0278	No
2008 FH	54556	1.5849644	0.50476518	3.46186	5.20388	264.09916	2.00	0.78	2.38	25	12	24.30	0.9982	0.0148	0.4663	0.0281	No
7753 (1988 XB)	57000	1.4676278	0.48187294	3.12289	73.46351	279.99693	1.78	0.76	2.17	804	9214	18.60	0.6570	0.0211	0.2292	0.0283	Yes
2008 EF <sub>32</sub>	54536	1.6276459	0.52218191	1.73604	349.17686	112.26942	2.08	0.78	2.48	8	1	29.40	0.2251	0.0391	0.0756	0.0295	No
2010 CJ <sub>1</sub>	55239	1.5642628	0.49482798	4.08833	138.17344	281.78334	1.96	0.79	2.34	26	7	24.10	0.1950	0.0219	0.0663	0.0319	No
2015 FB <sub>118</sub>	57000	1.4929421	0.46800607	5.12417	0.04734	106.45800	1.82	0.79	2.19	46	18	23.70	0.2583	0.0477	0.0895	0.0322	No
2011 EO <sub>40</sub>	57000	1.6540887	0.54016233	3.36286	50.30284	17.07473	2.13	0.76	2.55	20	34	21.50	0.1227	0.0429	0.0549	0.0331	Yes
2004 RN <sub>251</sub>	57000	1.6558104	0.52789965	4.39200	179.60954	245.93613	2.13	0.78	2.53	27	2	26.10	0.1663	0.0347	0.0634	0.0335	No
2007 DL <sub>41</sub>	57000	1.4566432	0.47649121	4.66517	150.81240	140.11206	1.76	0.76	2.15	112	2831	20.70	0.9424	0.0315	0.3958	0.0335	Yes
2012 TP <sub>139</sub>	57000	1.4675833	0.46485745	2.34197	271.85697	3.26339	1.78	0.79	2.15	103	476	20.30	0.9527	0.0418	0.4328	0.0340	Yes
2015 CC <sub>1</sub>	57070	1.5467360	0.51434097	3.59953	88.60772	327.84872	1.92	0.75	2.34	22	16	23.88	0.2085	0.0256	0.0704	0.0346	No
2010 DU <sub>1</sub>	55247	1.6892222	0.54017890	3.70925	147.83081	74.25332	2.20	0.78	2.60	22	4	26.50	1.0014	0.0419	0.4221	0.0383	No
2013 BR <sub>15</sub>	56309	1.5546110	0.52043752	1.95468	102.89879	284.89340	1.94	0.75	2.36	10	2	25.00	0.4305	0.0431	0.1439	0.0390	No
2014 RA	57000	1.4613373	0.45645528	3.12927	158.00395	108.93260	1.77	0.79	2.13	30	2	28.90	0.9593	0.0485	0.4491	0.0456	No
2005 EQ <sub>95</sub>	53440	1.6532901	0.52361268	2.37240	196.53230	251.80518	2.13	0.79	2.52	17	2	23.40	0.1447	0.0355	0.0544	0.0459	No
2011 GP <sub>28</sub>	57000	1.5046701	0.50455345	3.81544	16.27364	256.42378	1.85	0.75	2.26	14	1	29.40	0.9951	0.0272	0.4572	0.0463	No
2015 AM <sub>45</sub>	57000	1.5512258	0.51739809	5.58246	275.22926	107.47502	1.93	0.75	2.35	46	48	22.10	0.4651	0.0469	0.1549	0.0488	No

Table 7: Similar to Table 4 but for SOL2. Data as of 2015 August 19. Source: JPL Small-Body Database

Asteroid	Epoch	$a$ (AU)	$e$	$i$ (deg)	$\Omega$ (deg)	$\omega$ (deg)	$P_{\text{orb}}$ (year)	$q$ (AU)	$Q$ (AU)	$n$	arc (d)	$H$ (mag)	$D_{\text{SH}}$	$D_{\text{LS}}$	$D_{\text{D}}$	$D_{\text{R}}$	PHA
2002 CD <sub>14</sub>	57000	1.7779481	0.57944354	2.88679	127.69502	141.21700	2.37	0.75	2.81	47	2549	20.60	1.1519	0.0334	0.5314	0.0088	Yes
2013 UX	57000	1.6994971	0.56023315	5.44902	259.54850	51.72108	2.22	0.75	2.65	53	42	22.00	1.0067	0.0171	0.3920	0.0110	No
2006 WZ <sub>3</sub>	57000	1.7461625	0.57727458	3.81294	176.32213	0.30728	2.31	0.74	2.75	97	203	20.20	0.8975	0.0199	0.3247	0.0124	No
2009 SD	55091	1.7343896	0.56682933	3.04789	344.32550	287.05721	2.28	0.75	2.72	24	3	25.40	1.1293	0.0304	0.5207	0.0128	No
2012 FO <sub>35</sub>	57000	1.8096120	0.57922717	7.15565	179.36210	93.27960	2.43	0.76	2.86	27	15	23.60	1.1564	0.0445	0.5148	0.0134	No
2012 VA <sub>20</sub>	57000	1.6822360	0.55511183	4.39092	62.74253	240.11893	2.18	0.75	2.62	16	10	22.80	1.0416	0.0183	0.4194	0.0137	No
2002 AC <sub>9</sub>	57000	1.7038247	0.56051693	2.28428	2.58887	28.42304	2.22	0.75	2.66	51	3132	21.00	0.4367	0.0447	0.1432	0.0138	Yes
2014 KW <sub>76</sub>	57000	1.6825498	0.56131222	2.33519	67.46190	102.00097	2.18	0.74	2.63	34	4	27.90	0.8315	0.0447	0.2958	0.0154	No
2014 HQ <sub>4</sub>	57000	1.7502026	0.57583344	6.05533	210.72680	278.76893	2.32	0.74	2.76	20	4	26.20	0.5438	0.0237	0.1813	0.0166	No
159677 (2002 HQ <sub>11</sub> )	57000	1.8503734	0.59582251	6.04797	153.33514	322.13054	2.52	0.75	2.95	148	3817	19.40	0.4387	0.0327	0.1457	0.0198	No
2015 NU <sub>13</sub>	57220	1.8373112	0.58981322	4.20157	140.11078	259.77306	2.49	0.75	2.92	21	10	19.23	0.3922	0.0208	0.1305	0.0200	Yes
2013 OW <sub>2</sub>	57000	1.8307041	0.59311032	6.50010	221.75879	336.76736	2.48	0.74	2.92	22	28	21.10	1.0357	0.0371	0.4010	0.0215	No
358471 (2007 NS <sub>4</sub> )	57000	1.8747202	0.59757148	5.80175	11.23176	47.25005	2.57	0.75	2.99	83	2061	19.10	0.1945	0.0319	0.0654	0.0227	Yes
2001 WM <sub>15</sub>	52239	1.8653862	0.59394567	5.41106	244.20729	250.90778	2.55	0.76	2.97	34	4	25.00	0.5903	0.0262	0.1982	0.0241	No
2005 TE	53646	1.7473215	0.57690200	6.48704	13.07234	270.57774	2.31	0.74	2.76	17	6	23.90	1.1191	0.0318	0.4871	0.0243	No
1996 VB <sub>3</sub>	50401	1.6259062	0.54444404	2.79583	180.62271	132.68222	2.07	0.74	2.51	21	9	22.40	0.9877	0.0447	0.3823	0.0265	No
86039 (1999 NC <sub>43</sub> )	57000	1.7595889	0.57919044	7.12356	311.81453	120.57423	2.33	0.74	2.78	891	5492	16.00	0.0606	0.0426	0.0211	0.0269	Yes
2011 GZ <sub>2</sub>	57000	1.8367961	0.58046296	6.99505	18.57475	247.21411	2.49	0.77	2.90	51	6	26.10	1.1529	0.0459	0.5460	0.0290	No
267729 (2003 FC <sub>5</sub> )	57000	1.9167576	0.60910814	5.82513	189.25854	270.65349	2.65	0.75	3.08	629	4716	18.30	0.3035	0.0414	0.1062	0.0291	Yes
199801 (2007 AE <sub>12</sub> )	57000	1.6843105	0.56995521	2.28470	245.70900	86.67112	2.19	0.72	2.64	138	4995	19.50	0.9009	0.0493	0.3294	0.0326	Yes
2014 TM <sub>35</sub>	56948	1.9283432	0.60990027	3.20973	215.35752	87.14549	2.68	0.75	3.10	40	13	23.70	1.0920	0.0465	0.4390	0.0333	No
2008 EW <sub>84</sub>	54538	1.7504903	0.58321185	5.34640	170.56633	82.95460	2.32	0.73	2.77	16	2	24.50	1.1682	0.0239	0.5483	0.0333	No
2011 EO <sub>40</sub>	57000	1.6540887	0.54016233	3.36286	50.30284	17.07473	2.13	0.76	2.55	20	34	21.50	0.1323	0.0421	0.0516	0.0336	Yes
2007 EZ	57000	1.7070245	0.57260188	5.81095	98.52168	357.87061	2.23	0.73	2.68	111	3078	19.80	0.2636	0.0261	0.0865	0.0365	No
2010 TV <sub>54</sub>	57000	1.9133256	0.61405795	6.18704	202.37865	254.99077	2.65	0.74	3.09	31	6	25.70	0.2831	0.0497	0.1015	0.0374	No
2012 BC <sub>77</sub>	57000	1.8889272	0.59441053	4.60747	149.04739	58.14416	2.60	0.77	3.01	26	9	25.10	1.0757	0.0287	0.4266	0.0402	No
2011 GC <sub>55</sub>	57000	1.8242312	0.58019970	2.77258	98.96323	22.41153	2.46	0.77	2.88	62	24	23.00	0.4612	0.0397	0.1512	0.0413	No
2012 PS <sub>4</sub>	57000	1.7676567	0.59240205	3.93689	86.25805	144.14991	2.35	0.72	2.81	67	36	21.20	1.1437	0.0370	0.4995	0.0419	Yes
2010 TW <sub>149</sub>	55484	1.8922324	0.61598905	4.57001	195.85511	103.38629	2.60	0.73	3.06	20	1	25.90	1.1146	0.0488	0.4524	0.0434	No
220839 (2004 VA)	57000	1.9004546	0.59634469	3.69800	109.66945	43.10495	2.62	0.77	3.03	333	4076	17.30	0.7398	0.0358	0.2538	0.0462	Yes
2008 UT <sub>95</sub>	57000	1.8149119	0.57453004	3.81156	220.04223	247.43235	2.45	0.77	2.86	32	2	27.40	0.3366	0.0293	0.1114	0.0480	No

Table 8: Similar to Table 4 but for SOL3. Data as of 2015 August 19. Source: JPL Small-Body Database

Asteroid	Epoch	$a$ (AU)	$e$	$i$ (deg)	$\Omega$ (deg)	$\omega$ (deg)	$P_{\text{orb}}$ (year)	$q$ (AU)	$Q$ (AU)	$n$	arc (d)	$H$ (mag)	$D_{\text{SH}}$	$D_{\text{LS}}$	$D_{\text{D}}$	$D_{\text{R}}$	PHA
2013 OW <sub>2</sub>	57000	1.8307041	0.59311032	6.50010	221.75879	336.76736	2.48	0.74	2.92	22	28	21.10	1.0592	0.0225	0.4099	0.0011	No
159677 (2002 HQ <sub>11</sub> )	57000	1.8503734	0.59582251	6.04797	153.33514	322.13054	2.52	0.75	2.95	148	3817	19.40	0.4514	0.0158	0.1490	0.0084	No
2010 TV <sub>54</sub>	57000	1.9133256	0.61405795	6.18704	202.37865	254.99077	2.65	0.74	3.09	31	6	25.70	0.2906	0.0236	0.0997	0.0151	No
2014 HQ <sub>4</sub>	57000	1.7502026	0.57583344	6.05533	210.72680	278.76893	2.32	0.74	2.76	20	4	26.20	0.5591	0.0254	0.1872	0.0156	No
2006 WZ <sub>3</sub>	57000	1.7461625	0.57727458	3.81294	176.32213	0.30728	2.31	0.74	2.75	97	203	20.20	0.9194	0.0321	0.3329	0.0168	No
267729 (2003 FC <sub>5</sub> )	57000	1.9167576	0.60910814	5.82513	189.25854	270.65349	2.65	0.75	3.08	629	4716	18.30	0.3124	0.0181	0.1061	0.0172	Yes
86039 (1999 NC <sub>43</sub> )	57000	1.7595889	0.57919044	7.12356	311.81453	120.57423	2.33	0.74	2.78	891	5492	16.00	0.0565	0.0371	0.0231	0.0175	Yes
2005 TE	53646	1.7473215	0.57690200	6.48704	13.07234	270.57774	2.31	0.74	2.76	17	6	23.90	1.1428	0.0294	0.4973	0.0181	No
358471 (2007 NS <sub>4</sub> )	57000	1.8747202	0.59757148	5.80175	11.23176	47.25005	2.57	0.75	2.99	83	2061	19.10	0.1956	0.0171	0.0630	0.0214	Yes
2010 TW <sub>149</sub>	55484	1.8922324	0.61598905	4.57001	195.85511	103.38629	2.60	0.73	3.06	20	1	25.90	1.1367	0.0263	0.4596	0.0215	No
2008 EW <sub>84</sub>	54538	1.7504903	0.58321185	5.34640	170.56633	82.95460	2.32	0.73	2.77	16	2	24.50	1.1939	0.0175	0.5588	0.0231	No
2012 FO <sub>35</sub>	56013	1.8096120	0.57922717	7.15565	179.36210	93.27960	2.43	0.76	2.86	27	15	23.60	1.1818	0.0432	0.5248	0.0236	No
2002 CD <sub>14</sub>	57000	1.7779481	0.57944354	2.88679	127.69502	141.21700	2.37	0.75	2.81	47	2549	20.60	1.1772	0.0455	0.5419	0.0250	Yes
2013 VX <sub>13</sub>	56610	1.9595239	0.62550101	6.14648	17.37851	301.55846	2.74	0.73	3.19	24	14	22.10	1.0461	0.0331	0.3988	0.0252	No
2009 MG <sub>1</sub>	55007	2.0038233	0.62552004	6.79624	87.89116	101.43854	2.84	0.75	3.26	19	11	24.00	1.0385	0.0405	0.3882	0.0262	No
2012 SV <sub>9</sub>	56190	2.0097244	0.63303198	4.79202	188.73213	80.70820	2.85	0.74	3.28	18	5	23.90	1.2324	0.0370	0.5610	0.0263	No
2015 NU <sub>13</sub>	57220	1.8373112	0.58981322	4.20157	140.11078	259.77306	2.49	0.75	2.92	21	10	19.23	0.4006	0.0239	0.1332	0.0277	Yes
2013 UX	57000	1.6994971	0.56023315	5.44902	259.54850	51.72108	2.22	0.75	2.65	53	42	22.00	1.0285	0.0376	0.4009	0.0280	No
2001 WM <sub>15</sub>	52239	1.8653862	0.59394567	5.41106	244.20729	250.90778	2.55	0.76	2.97	34	4	25.00	0.6054	0.0177	0.2028	0.0284	No
2012 PS <sub>4</sub>	57000	1.7676567	0.59240205	3.93689	86.25805	144.14991	2.35	0.72	2.81	67	36	21.20	1.1687	0.0307	0.5100	0.0284	Yes
2012 HD <sub>25</sub>	56046	1.9765398	0.63026934	5.95173	42.63974	93.21000	2.78	0.73	3.22	47	5	23.60	0.6255	0.0367	0.2094	0.0296	No
303449 (2005 BE <sub>2</sub> )	57000	2.0152022	0.62594237	6.57681	92.63080	162.40881	2.86	0.75	3.28	276	3600	18.20	1.2371	0.0394	0.5912	0.0303	No
2007 EZ	57000	1.7070245	0.57260188	5.81095	98.52168	357.87061	2.23	0.73	2.68	111	3078	19.80	0.2742	0.0283	0.0917	0.0309	No
2014 TM <sub>35</sub>	56948	1.9283432	0.60990027	3.20973	215.35752	87.14549	2.68	0.75	3.10	40	13	23.70	1.1139	0.0398	0.4464	0.0323	No
2012 VA <sub>20</sub>	57000	1.6822360	0.55511183	4.39092	62.74253	240.11893	2.18	0.75	2.62	16	10	22.80	1.0649	0.0453	0.4294	0.0346	No
2002 VR <sub>85</sub>	57000	1.8169080	0.60420879	6.01821	204.85943	298.80545	2.45	0.72	2.91	59	29	20.40	0.6955	0.0260	0.2363	0.0382	Yes
2011 GZ <sub>2</sub>	57000	1.8367961	0.58046296	6.99505	18.57475	247.21411	2.49	0.77	2.90	51	6	26.10	1.1777	0.0460	0.5576	0.0399	No
4183 Cuno (1959 LM)	57000	1.9822062	0.63441443	6.70752	294.93347	236.27353	2.79	0.72	3.24	1645	20497	14.40	0.9159	0.0478	0.3296	0.0414	Yes
2015 PK	57000	1.9296505	0.59917954	7.21027	133.28762	111.31405	2.68	0.77	3.09	26	1	28.14	1.2104	0.0476	0.5496	0.0458	No
2013 EB <sub>34</sub>	56364	1.8594018	0.61304902	7.33262	160.04942	96.99762	2.54	0.72	3.00	20	4	24.70	1.2297	0.0447	0.5682	0.0460	No
2013 EF <sub>68</sub>	56365	1.9812035	0.63801017	5.56067	177.16206	277.12496	2.79	0.72	3.25	28	1	25.80	0.2751	0.0474	0.1003	0.0462	No
2013 VW <sub>13</sub>	57000	1.6726846	0.57435835	3.52659	227.74983	101.32453	2.16	0.71	2.63	34	21	26.20	0.9463	0.0472	0.3488	0.0480	No
2012 BC <sub>77</sub>	57000	1.8889272	0.59441053	4.60747	149.04739	58.14416	2.60	0.77	3.01	26	9	25.10	1.1002	0.0284	0.4360	0.0482	No
2014 TK <sub>64</sub>	56948	1.9634840	0.60692881	6.72030	16.22175	88.43995	2.75	0.77	3.16	17	7	23.30	0.3141	0.0418	0.1030	0.0484	No

## 7. Discussion and conclusions

In this paper, we have obtained a statistically robust solution for the pre-impact orbit of the Chelyabinsk impactor. This solution has been computed by making use of full  $N$ -body calculations and it reproduces, within very narrow limits ( $<0.0001\%$  in time and  $<0.4\%$  in position), the well documented values of both impact time and location of the Chelyabinsk event. It is compatible with other observational properties as well. The impact probability of our solution is  $> 99.999\%$  and it is consistent with those in Papers I and II although the methodology behind it is completely different. It also matches well the one originally computed by S. Nakano:<sup>5</sup> relative differences of  $0.14\%$  in  $a$ ,  $0.14\%$  in  $e$ ,  $2.7\%$  in  $i$ ,  $0.011\%$  in  $\Omega$ , and  $0.007\%$  in  $\omega$ . Our simulations also confirm the existence of a reasonably strong dynamical link between the PHA 2011 EO<sub>40</sub> and the Chelyabinsk impactor as described by the solution in Table 2. Alternative, relevant candidate solutions are also explored. Our statistical analysis shows that the value of the geocentric velocity of the impactor at the entry point in the atmosphere is currently the key limiting parameter to obtaining a robust and final determination of the orbital solution of the Chelyabinsk asteroid. Further work may be required in that respect. On the other hand, our study vindicates the role of quality control based on  $N$ -body-integrations in the determination of pre-impact meteor orbits. Without such quality control, orbital solutions may be meaningless as they do not produce any relevant impacts. A statistical analysis should be standard practice in these cases.

Borovička et al. (2013) suggested that the Chelyabinsk impactor and the PHA 86039 (1999 NC<sub>43</sub>) were once part of the same object. Reddy et al. (2015) later pointed out that the existence of a connection between the Chelyabinsk meteoroid and 86039 is very weak, both in dynamical and compositional terms. Here, we lend further support to this conclusion. Our extensive simulations show that it is highly unlikely that, prior to colliding with our planet, the Chelyabinsk impactor followed an orbit similar to the ones described in Borovička et al. (2013) or Popova et al. (2013). In both cases, their orbital solutions are unable to place the impactor sufficiently close to our planet within 10 or less minutes of the well documented value of the impact time, which is consistent with our analysis in Paper II.

On 1908 June 30 a small body was observed streaking across the daytime sky in a remote part of Russia, above the Tunguska River. The subsequent meteor airburst, known as the Tunguska event, is considered the most powerful asteroid impact witnessed to date (see, e.g., Farinella et al. 2001). Almost 107 years later, the Chelyabinsk event has become the second most powerful instance of an observed meteor airburst (Brown et al. 2013; Le Pichon et al. 2013). In both cases, the glare of the Sun provided an effective hiding spot to the eventual impactor, highlighting the fact that these objects are still a challenge for our modern resources. However, asteroids impacting from the direction of the Sun are probably no different from those impacting at opposition (Hills & Leonard 1995) although they could form more than 30% of the NEOs (Isobe & Yoshikawa 1997) and are better detected from spaceborne telescopes, perhaps located at the L<sub>2</sub> point or orbiting Venus (Hills 1992; Hills & Leonard 1995). A number of initiatives in that direction have been discussed recently (e.g., Dunham et al. 2013; Mainzer et al. 2015).

We thank the anonymous referee for a constructive and helpful report, E. Schunová for her feedback on earlier versions of this manuscript, S. D. Miller for comments on his results, and P. Wiegert for sharing the details of his pre-impact orbital solution. This work was partially supported by the Spanish “Comunidad de Madrid” under grant CAM S2009/ESP-1496. Some of the calculations discussed here were completed on the “Servidor Central de Cálculo” of the Universidad Complutense de Madrid. In the preparation of this paper, we made use of the NASA Astrophysics Data System, the ASTRO-PH e-print server, the MPC data server, and the NEODyS information service.

## REFERENCES

- Aarseth, S. J. 2003, *Gravitational N-body simulations* (Cambridge: Cambridge Univ. Press)
- Adamo, D. R. 2011, *Horizons Newsletter*, June 2011, p. 64
- Adamo, D. R. 2013, *Horizons Newsletter*, March/April 2013, p. 28
- Avdyushev, V. A., & Banschikova, M. A. 2007, *SoSyR.*, 41, 413
- Boekholt, T., & Portegies Zwart, S. 2015, *ComAC*, 2, 2
- Bordovitsyna, T., Avdyushev, V., & Chernitsov, A. 2001, *CeMDA*, 80, 227
- Borovička, J., Spurný, P., Brown, P., et al. 2013, *Natur*, 503, 235
- Bottke, W. F., Jr., Vokrouhlický, D., Rubincam, D. P., Nesvorný, D. 2006, *ARE&PS*, 34, 157
- Brown, P. G., Assink, J. D., Astiz, L., et al. 2013, *Natur*, 503, 238
- Chodas, P. W. 1999, *BAAS*, 31, 1117
- de la Fuente Marcos, C., & de la Fuente Marcos, R. 2012, *MNRAS*, 427, 728
- de la Fuente Marcos, C., & de la Fuente Marcos, R. 2013, *MNRAS*, 436, L15 (Paper I)
- de la Fuente Marcos, C., & de la Fuente Marcos, R. 2014, *MNRAS*, 443, L39 (Paper II)
- de la Fuente Marcos, C., & de la Fuente Marcos, R. 2015, *MNRAS*, 453, 1288
- de León, J., Pinilla-Alonso, N., Ortiz, J., et al. 2013, *A&A*, 555, L2
- Dmitriev, V., Lupovka, V., & Gritsevich, M. 2015, *P&SS*, in press (doi: 10.1016/j.pss.2015.06.015)
- Drummond, J. D. 1981, *Icar*, 45, 545
- Dunham, D. W., Reitsema, H. J., Lu, E., et al. 2013, *SoSyR*, 47, 315

- Emel'Yanenko, V. V., Naroenkov, S. A., Jenniskens, P., & Popova, O. P. 2014, *M&PS*, 49, 2169
- Farinella, P., Foschini, L., Froeschlé, C., et al. 2001, *A&A*, 377, 1081
- Farnocchia, D., Chesley, S. R., Vokrouhlický, D., et al. 2013, *Icar*, 224, 1
- Giorgini, J. D., Yeomans, D. K., Chamberlin, A. B., et al. 1996, *BAAS*, 28, 1158
- Gladman, B. J., Migliorini, F., Morbidelli, A., et al. 1997, *Sci*, 277, 197
- Golubaev, A. V. 2015, *SoSyR*, 49, 147
- Green, D. W. E. 2013, *Cent. Bur. Electron. Telegrams*, 3423, 1
- Hills, J. G. 1992, in *Proceedings of the Near-Earth-Object Interception Workshop*, ed. G. H. Canavan, J. C. Solem, & J. D. G. Rather, Los Alamos National Laboratory Publication LA-12476-C, pp. 20
- Hills, J. G., & Leonard, P. J. T. 1995, *AJ*, 109, 401
- Isobe, S., & Yoshikawa, M. 1997, in *Near-Earth Objects, the United Nations International Conference*, ed. J. L. Remo, NYASA, 822, 140
- Jenniskens, P. 2006, *Meteor Showers and Their Parent Comets* (Cambridge: Cambridge Univ. Press)
- Lai, H., Russell, C. T., Wei, H., & Zhang, T. 2014, *M&PS*, 49, 28
- Le Pichon, A., Ceranna, L., Pilger, C., et al. 2013, *GeoRL*, 40, 3732
- Lindblad, B. A., & Southworth, R. B. 1971, in *Physical Studies of Minor Planets*, ed. T. Gehrels, NASA SP-267, pp. 337
- Mainzer, A., Grav, T., Bauer, J., et al. 2015, *AJ*, 149, 172
- Makino, J. 1991, *ApJ*, 369, 200
- Metropolis, N., & Ulam, S. 1949, *J. Am. Stat. Assoc.*, 44, 335
- Milani, A., Chesley, S. R., & Valsecchi, G. B. 1999, *A&A*, 346, L65
- Miller, S. D., Straka, W. C. III, Bachmeier, A. S., et al. 2013, *PNAS*, 110, 18092
- Morbidelli, A., Gonczi, R., Froeschlé, C., & Farinella, P. 1994, *A&A*, 282, 955
- Murray, C. D., & Dermott, S. F. 1999, *Solar System Dynamics* (Cambridge: Cambridge Univ. Press)
- Nechaeva, M., Antipenko, A., Bezrukov, D., et al. 2013, *BaltA*, 22, 341

- Olech, A., Zoladek, P., Wisniewski, M., et al. 2015, MNRAS, in press (eprint arXiv:1507.08459)
- Pauls, A., & Gladman, B. 2005, M&PS, 40, 1241
- Popova, O. P., Jenniskens, P., Emel'Yanenko, V., et al. 2013, Sci, 342, 1069
- Press, W. H., Teukolsky, S. A., Vetterling, W. T., & Flannery, B. P. 2007, Numerical Recipes: The Art of Scientific Computing, 3rd Edition (Cambridge: Cambridge Univ. Press)
- Proud, S. R. 2013, GeoRL, 40, 3351
- Reddy, V., Vokrouhlický, D., Bottke, W. F., et al. 2015, Icar, 252, 129
- Rubin, A. E., & Matson, R. D. 2008, EM&P, 103, 73
- Scholl, H., & Froeschlé, C. 1991, A&A, 245, 316
- Schunová, E., Granvik, M., Jedicke, R., et al. 2012, Icar, 220, 1050
- Schunová, E., Jedicke, R., Walsh, K. J., et al. 2014, Icar, 238, 156
- Sitarski, G. 1998, AcA, 48, 547
- Sitarski, G. 1999, AcA, 49, 421
- Sitarski, G. 2006, AcA, 56, 283
- Southworth, R. B., & Hawkins, G. S. 1963, SCoA, 7, 261
- Standish, E. M. 1998, JPL Planetary and Lunar Ephemerides, DE405/LE405, Interoffice Memo. 312.F-98-048, NASA JPL
- Takahashi, J., Urakawa, S., Terai, T., et al. 2014, PASJ, 66, 53
- Terai, T., Urakawa, S., Takahashi, J., et al. 2013, A&A, 559, A106
- Terentjeva, A., & Bakanas, E. 2013, WGN, JIMO, 41, 39
- Trigo-Rodríguez, J. M., Lyytinen, E., Jones, D. C., et al. 2007, MNRAS, 382, 1933
- Unnikrishnan, R., Lalonde, J.-F., Vandapel, N., & Hebert, M. 2006, in Proceedings of 3DPVT'06 - The Third International Symposium on 3D Data Processing Visualization and Transmission, pp. 1026
- Unnikrishnan, R. 2008, PhD thesis, Carnegie Mellon University
- Unnikrishnan, R., Lalonde, J.-F., Vandapel, N., & Hebert, M. 2010, Int. J. Comput. Geom. Appl., 20, 543
- Urakawa S., Fujii M., Hanayama H., et al. 2013, PASJ, 65, L9

Valsecchi, G. B., Jopek, T. J., & Froeschlé, C. 1999, *MNRAS*, 304, 743

Vokrouhlický, D., Farnocchia, D., Čapek, D., et al. 2015, *Icar*, 252, 277

Włodarczyk, I. 2012, *MNRAS*, 427, 1175

Zuluaga, J. I., Ferrin, I., & Geens, S. 2013, *E&PSL*, preprint (arXiv:1303.1796)

**A. Cartesian state vectors at epoch JDCT 2456337.63888889 = A.D. 2013  
February 14 03:20:00.0000 UTC**

In order to facilitate verification of our results by other astrodynamacists, we show in Table 9 the Cartesian state vectors of the physical model used in all the calculations presented here. These values have been computed by the SSDG, Horizons On-Line Ephemeris System at epoch JDCT 2456337.63888889 = A.D. 2013 February 14 03:20:00.0000 UTC; this instant is considered as  $t = 0$  across this work unless explicitly stated. Positions and velocities are referred to the barycenter of the solar system.

Table 9: Cartesian State Vectors at Epoch JDCT 2456337.63888889 = A.D. 2013 February 14 03:20:00.0000 UTC (Source: JPL HORIZONS System, Data as of 2015 April 27)

Body	Mass (kg)	X (AU)	Y (AU)	Z (AU)	$V_X$ (AU/day)	$V_Y$ (AU/day)	$V_Z$ (AU/day)
Sun	1.988544D+30	-1.011494946041879D-03	-2.504114162880022D-03	-4.792865115835242D-05	6.220894815132611D-06	-8.990667125614989D-07	-1.353378656456761D-07
Mercury	3.302D+23	1.601238578327888D-01	2.625722472443697D-01	6.825890471667526D-03	-2.964378655400363D-02	1.573883688706671D-02	4.006348641371026D-03
Venus	48.685D+23	3.684190336612509D-01	-6.292530937012436D-01	-2.995683700834373D-02	1.729515787108521D-02	1.019957367549420D-02	-8.581635029629278D-04
Earth	5.97219D+24	-8.140698930244055D-01	5.581120070644801D-01	-6.589763331176098D-05	-1.003900706480297D-02	-1.423531287380917D-02	7.820902130810397D-07
Moon	734.9D+20	-8.115470135393000D-01	5.587246391320240D-01	7.135598656712641D-05	-1.014006812230196D-02	-1.366171847421980D-02	-3.819647952433072D-05
Mars	6.4185D+23	1.358696919954038D+00	-2.609405990577065D-01	-3.884700972410955D-02	3.155433071794785D-03	1.494047053495886D-02	2.355938303052990D-04
(1) Ceres	8.958D+20	-4.530641758590559D-01	2.582498614052824D+00	1.645168996062354D-01	-1.039618361109546D-02	-2.573247707241392D-03	1.837093277694028D-03
(2) Pallas	2.108D+20	2.14872237773673D+00	1.139324612315395D+00	-9.682180658594401D-01	-8.045289972243500D-03	6.359998630354690D-03	-3.724517164654106D-03
(4) Vesta	2.59076D+20	-1.208190498587545D-01	2.553051597561101D+00	-6.210372692193103D-02	-1.018543503227075D-02	-7.531638828710834D-04	1.261808261070763D-03
(10) Hygiea	8.67D+19	3.292138218259053D+00	-7.753641456595389D-02	2.138959793656113D-01	1.160053746471100D-03	9.141540670241449D-03	2.177016629356885D-04
(31) Euphrosyne	5.81D+19	-2.602099194748581D+00	5.537190212892845D-01	9.009030329104319D-01	-5.116957924612657D-03	-9.168433478330714D-03	-2.569751792414020D-03
Jupiter	1898.13D+24	1.097408567386605D+00	4.954902903200203D+00	-4.521676703255616D-02	-7.458634311741788D-03	1.992263681815774D-03	1.586575650167676D-04
Saturn	5.68319D+26	-7.954280583549062D+00	-5.719387687644644D+00	4.160061774451558D-01	2.953857543128144D-03	-4.543457016907906D-03	-3.820665181298168D-05
Uranus	86.8103D+24	1.986481516054372D+01	2.734885430030593D+00	-2.472007163305052D-01	-5.653198932594880D-04	3.713021339159490D-03	2.101603062461898D-05
Neptune	102.41D+24	2.662268720316427D+01	-1.380194387354347D+01	-3.293215144108281D-01	1.424320769695806D-03	2.805857995688192D-03	-9.052868025176624D-05
Pluto-Charon barycenter	1.45712D+22	5.247177290509663D+00	-3.190345013616387D+01	1.896073175017724D+00	3.157371987049258D-03	-1.182716627674995D-04	-9.006421307059045D-04
Nominal impactor	1.0D+07	-8.0679626173D-01	5.5488529365D-01	1.29912462D-03	-1.726521543D-02	-1.104192256D-02	-1.30271852D-03

Note. The sample Cartesian vector for the Chelyabinsk impactor corresponds to the nominal orbit in Table 2.